

**IMPERFECTIONS ON THE STABILITY OF REUSED STEEL
STRUCTURES**



Bachelor's thesis

Visamäki Campus, Degree Programme in Construction Engineering

Autumn semester 2020

Chenjie Ruan

Construction engineering
Visamäki

Author	Chenjie Ruan	Year 2020
Subject	Imperfections on the Stability of reused Steel Structures	
Supervisor(s)	Zhongcheng Ma	

ABSTRACT

Steel is a recyclable building material. Although there are some buildings built with reused steel structures around the world, there is no clear international standard for the performance of reused steel structures. It will be much more convenient and has a great contribution to environmental protection if the design rules for reused steel structures are obtained by a series of theoretical and experimental investigations. Therefore, the research objective of this thesis is the reused steel structures, and the subject is the Effects of Imperfections on the Stability of Reused Steel Structures.

The purpose of this thesis is to summarize how to measure the residual stresses due to re-fabrications and geometric deformation on steel components after deconstruction and reconstruction through the method of literature review, and perform preliminary finite element analysis in ABAQUS to check the influence of imperfections on the stability of steel members using nonlinear buckling analysis.

Keywords Residual stress, geometric imperfection, reused steel structures, finite element analysis, nonlinear buckling analysis

Pages 65 pages including appendices 15 pages

CONTENTS

1	INTRODUCTION	1
2	INTRODUCTION OF REUSED STEEL	2
3	LITERATURE REVIEW OF RESIDUAL STRESS.....	3
3.1	Definition of residual stresses	3
3.2	Effect of residual stresses	4
3.2.1	Effect on yield limit.....	4
3.2.2	Effect on component deformation.....	4
3.2.3	Effect on various properties of components.....	5
3.3	Residual stress measurement method.....	5
3.3.1	Mechanical methods	5
3.3.2	Diffraction methods.....	5
3.4	Basic hole-drilling method to measure residual stress	6
3.4.1	Basic drilling method	6
3.4.2	Incremental hole-drilling method	8
3.4.3	Apparatus preparation and technology	10
3.4.4	Drilling technology.....	12
3.4.5	Calculation methods.....	13
3.4.6	integral method	13
3.5	sectioning method to measure residual stress	16
3.5.1	Sample preparation	17
3.5.2	Measurement	17
3.5.3	Calculation steps.....	19
4	LITERATURE REVIEW OF GEOMETRIC IMPERFECTION	20
4.1	Definition of geometric imperfection.....	20
4.2	The influence of geometric imperfection on steel structure	23
4.2.1	hot-rolled steel structures.....	23
4.2.2	Cold-formed steel structures.....	24
4.3	Geometric imperfection measurement	26
4.3.1	Measurement method of initial local geometric imperfections.....	26
4.3.2	Measurement method of initial global geometric imperfections.....	28
4.4	Geometric imperfection measurement of cold-formed steel.....	29
5	FINITE ELEMENT METHOD.....	34
5.1	Introduction of the ABAQUS	35
5.1.1	Finite element analysis process by ABAQUS	35
5.1.2	Commonly used function modules in ABAQUS.....	36
5.2	Assign imperfection and residual stress to model	37
5.3	beam buckling analysis.....	38
5.3.1	Purpose.....	38
5.3.2	Profile, loading, boundary condition of the component and research method	39
5.3.3	Process.....	40

5.3.4 Results and Discussions	44
6 CONCLUSION	48
REFERENCES.....	49

Appendices

Appendix 1 RESULTS OF BUCKLING ANALYSIS IN ABAQUS

Appendix 2 LATERAL TORSIONAL BUCKLING RESISTANCE CALCULATION

1 INTRODUCTION

Steel is a durable building material. Although there are some buildings built with reused steel structures around the world, there is no clear international standard for the performance of reused steel structures. If a series of experimental and theoretical investigations are performed, and design rules and specifications are drawn based on the studies for reused components, a lot of resources can be saved in the future and great contribution to the environmental protection can be made. Therefore, the research objective of this thesis is the reused steel structures, and the subject is Effects of Imperfections on the Stability of Reused Steel Structures.

In order to study the effect of imperfections on the reused steel structures, some commonly used measurement methods for measuring residual stress in steel structures will be introduced, and some simple measurement methods that can measure geometric imperfections of components will also be selected.

Thanks to the rapid development of computer technology nowadays, many software that can be used to simulate structural behavior models are born. One software called ABAQUS is suitable for simulating the residual stresses and geometric imperfections of steel structures will be introduced in the text as well.

The purpose of this thesis is to summarize how to measure the residual stress and geometric deformation on steel components after deconstruction and reconstruction through the method of literature review, and have an introduction about finite element analysis software that can help people check the influence of imperfections on the stability of steel members.

2 INTRODUCTION OF REUSED STEEL

With the increasing global construction demand, the consumption of building materials is increasing. Nowadays, the construction environment consumes more than half of the global steel production, and the large-scale production of steel will bring greater challenges to the increasingly serious environmental problems. For this reason, it is particularly important to find a way to save materials and maintain natural balance.

Because steel is durable, it can be processed (bending, tearing, and other treatments) many times and still retain its value. Even if steel is mixed with other materials, it can be magnetically separated for recycling. Therefore, the reuse of steel is considered to be a good way to meet the requirements of people while reducing environmental impact.

The reuse of steel structures is not a new idea, on the contrary, it has become more and more common in the past few decades. However, due to various obstacles, the utilization rate of steel structure reuse has decreased. However, with the increasingly serious environmental problems, the construction industry is facing increasing pressure to improve resource utilization efficiency, reduce waste and reduce specific carbon impacts. Recently, especially at the EU, the concept of circular economy is being promoted and a road map has been developed to support the transition to a resource-saving, low-carbon European economy. Therefore, research on the reused steel structures has received more attention.

Most of the scrap steel from the demolition of buildings can be used in blast furnaces or electric furnaces to produce new materials. This new material is functionally the same as the original material. However, the melting, rolling and forming of recycled steel products consume a lot of energy and resources, and generate waste and emissions. In contrast, reused steel components are a better solution. The two existing large European projects REDUCE and PROGRESS are to achieve the goal of energy saving and emission reduction by reusing steel components.

3 LITERATURE REVIEW OF RESIDUAL STRESS

3.1 Definition of residual stresses

In EUROCODE 3, residual stress was defined as a permanent stress state in a static equilibrium state in a structure, independent of any applied effects. It can be grounded from the concept that the residual stress does not refer to a value of another distribution state or called the residual stress field. Residual stress is not only a compressive stress or tensile stress but also a balanced tensile or compressive stress. Residual stress is elastic stress, and theoretically its value should not exceed the yield strength of the material.

There are many reasons for the residual stress, but in most cases, it is caused by the geometric deformation of the component itself and the operation of the component during installation or production. For example, welding is a typical step that causes residual stress in steel components. In a broad sense, welding requires high temperature and high pressure to achieve permanent bonding between atoms. The contact surface of the two objects is in a molten state, while the other parts maintain the structural strength of the raw material with room temperature to form a welded structure. This will form an uneven temperature field in the welding area. After the welding is completed, due to the principle of thermal expansion and contraction, after cooling, the area with low temperature shrinks less, and the area with high temperature shrinks more, which will eventually lead to uneven deformation of the welded area, resulting in residual stress and geometric deformation.

The reason for using the above example is to prove that most of the residual stress of steel structure is caused by its production and processing methods, and understanding this is very helpful for the next analysis of why the residual stress in reused steel structure will increase.

3.2 Effect of residual stresses

3.2.1 Effect on yield limit

The existence of residual stress has many influences on steel components, the most important is the influence on the yield limit. As shown in the figure below, when the material has tensile residual stress, the actual tensile yield strength limit of the material will decrease, and the components that should yield at the yield strength limit will reach the yield limit earlier due to the influence of the residual stress. For instance, in the design of the column, if the residual stress in the member is not considered, the designed column's ability to bear the load may be overestimated, so that the structure cannot meet the requirements.

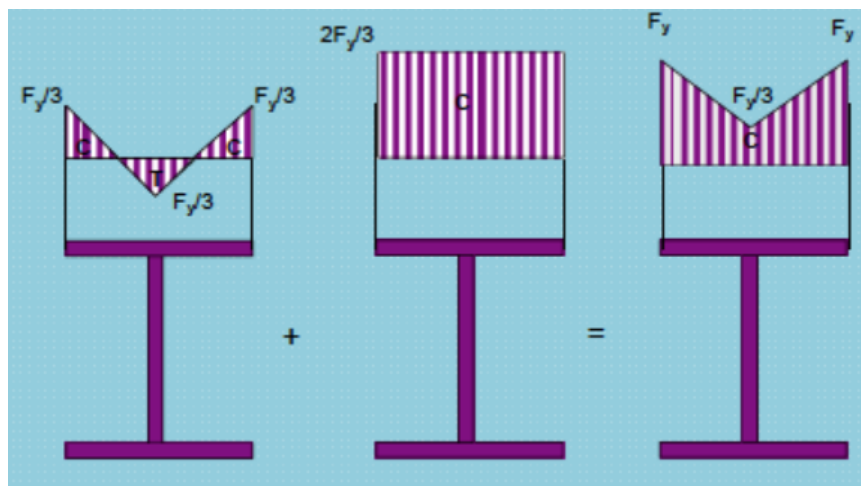


Figure 1. When the section force reaches the two-thirds yield limit

3.2.2 Effect on component deformation

Because of the uneven distribution of residual stress, some parts of the component will be plastically deformed when the external load is received. When the external load is removed, the entire component will be deformed due to the previous influence. The residual stress will affect the accuracy of the component after processing. Regarding the reused steel structures, special attention needs to be paid when removing the steel structures in the first life cycle, because in some possible removal steps such as cutting, the residual stress caused by high temperature may deform the components.

3.2.3 Effect on various properties of components

In addition to the effect on component deformation and yield limit, residual stress can also cause a series of reactions such as reducing component fatigue strength, corrosion resistance, and accelerating component brittle failure. These things were described in < Harmfulness of residual stress and countermeasures > made by FU Xue yi (1).

3.3 Residual stress measurement method

For reused steel structures, because the actual load borne during the first life cycle is difficult to define, the residual stress inside the structure is likely to change. Certain steps in the deconstruction of steel structures will also affect the residual stress of the steel structure, so after the completion of the demolition work, it is necessary to carry out the residual stress detection of the reused steel structure.

There are many methods for detecting residual stress of steel components, which can be divided into destructive testing and non-destructive testing according to whether the sample is damaged. The more commonly used methods at this stage are the mechanical strain gauge methods and the diffraction methods.

3.3.1 Mechanical methods

In mechanical methods, hole-drilling is a common method for detecting residual stress in metals. Although this method has been proposed by J. Mathar in 1932, under continuous improvement, this method is suitable for smaller thicknesses. The measurement accuracy of metal components is very good, and the damage to the metal in the destructive testing is small compared to the method of taking the strip, the method of notching and other methods that have great damage to the metal sample.

The Inherent strain method adopted by Ueda is a highly accurate measurement method that can accurately measure the residual stress of metals. The realization of this method requires qualified experimental conditions and highly specialized mechanical cutting equipment

3.3.2 Diffraction methods

Nowadays, there are two diffraction methods with high adoption rate, they are X-ray diffraction method and neutron diffraction method.

X-ray diffraction mainly uses the Bragg equation of crystal X-ray diffraction to determine the nature and magnitude of residual stress according to the shift direction and amplitude of crystal diffraction peaks. It belongs to non-destructive testing with high test accuracy. The disadvantage is that it can only complete the surface stress value test, and the thickness that can be measured is between a few microns to tens of microns depending on the material. Layer by layer peeling can be used to determine the deeper residual stress value of the component, but the peeling will affect the accuracy of the test results.

Neutron diffraction also uses the Bragg equation of crystal diffraction to calculate strain and then residual stress. However, compared with X-ray diffraction, the penetration layer of neutron diffraction is deeper. Aluminium alloy is 200mm and steel material is 80mm. Its advantage is that the residual stress inside the material can be measured in situ without damage. The disadvantage is that the measured value is the average stress in a larger area. It is difficult to accurately measure the residual stress gradient distribution, and the cost is high.

3.4 Basic hole-drilling method to measure residual stress

3.4.1 Basic drilling method

As shown in Figure 2, the method is to paste a special foil strain gauge on the surface of the component to be measured, and then drill a hole in the center of the strain gauge to achieve the purpose of stress release. The stress release produces strain, and the value is measured by the strain gauge, and then calculate the residual stress according to the elastic mechanics formula. The released strains depend on the stress originally present at the boundaries of the drilled hole(it is assumed that the residual stress acts uniformly in the in-plane area around the rosette and only changes in the thickness of the material).

The measurement accuracy of the hole-drilling method is mainly based on the displacement release coefficients A and B. The strain release coefficient can be calculated by Kirsch theory.

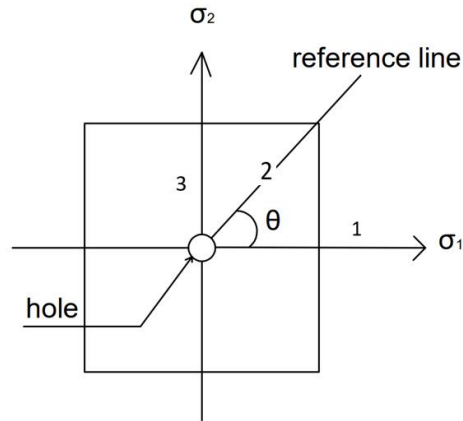


Figure 2. figure of drilling hole

The strain around the hole can be measured by mechanical length measurement, resistance strain gauges, etc. The calculation formulas for the average principal stress σ_1 and σ_2 and the principal stress direction angle θ within the hole depth are as follows:

$$\sigma_1 = (1/4A)(\varepsilon_1 + \varepsilon_2) + (1/4B)\sqrt{(\varepsilon_1 + \varepsilon_2)^2 + [2\varepsilon_2 - (\varepsilon_1 + \varepsilon_2)]^2}$$

$$\sigma_2 = (1/4A)(\varepsilon_1 + \varepsilon_3) - (1/4B)\sqrt{(\varepsilon_1 - \varepsilon_2)^2 + [2\varepsilon_2 - (\varepsilon_1 + \varepsilon_2)]^2}$$

$$\tan 2\theta = [(\varepsilon_1 + \varepsilon_3) - 2\varepsilon_2] / (\varepsilon_1 - \varepsilon_3)$$

In the formula, ε_1 , ε_2 , and ε_3 are the strain measured by the strain gauge respectively; A and B are the release coefficients.

The most important point of measuring residual stress with the hole-drilling method is the determination of the strain release coefficients A and B. The formula for the strain release coefficient based on Kirsch theory is as follows:

$$\begin{cases} A = -\frac{1+\mu}{E} \cdot \frac{a^2}{2r_1r_2} \\ B = \frac{2a^2}{Er_1r_2} \left[\frac{(1+\mu)a^2(r_1^2 + r_1r_2 + r_2^2)}{4r_1^2r_2^2} - 1 \right] \end{cases}$$

Where a is the diameter of the hole, r_1 and r_2 are the distances from the blind hole center to the near hole end and the far hole end of the strain gauge, respectively. E is the modulus of elasticity, μ is the Poisson's ratio.

The above formula refers to Li Wei-long's Test of residual stress by hole drilling strain method (15). they are derived under elastic deformation conditions. If the residual stress is close to or reaches the yield stress of

the material, and the stress around the hole exceeds the yield strength of the material due to drilling, and finally plastic deformation occurs, then the formula cannot be used directly at this time To calculate the strain release coefficient. In actual production, the strain release coefficient obtained by the calibration experiment is undoubtedly more accurate than the calculated one, but from an economic point of view, the calculation method is obviously more popular and convenient.

Regarding how to make a hole on a component, the simplest method is to use a drill hole to make a hole on the component. This method is simple to operate and the equipment is cheap. It only needs a drill bit and corresponding fixed equipment.

The more accurate method is to use the sandblasting hole method. The sandblast hole method requires a sandblasting punching device. It uses a rotating nozzle to aim at the center of the strain gauge to gradually corrode the hole. Compared with traditional drilling and opening, this method has a smaller cutting volume and can take away the heat generated by abrasion through the airflow produced by itself, so it will not cause too much processing strain and can greatly improve the measurement Accuracy. The disadvantage of this method is that it is not suitable for testing components with stress gradients.

3.4.2 Incremental hole-drilling method

The document AIAS –TR01:2010 (4) co-authored by A.Ajvalasit, M.Scafidi, B.Zuccarello, etc. describes the Incremental hole-drilling method in great detail, which is used as a reference.

Compared with the basic hole-drilling method, the incremental hole-drilling method can obtain the residual stress as a function of depth measured from the specimen surface. The plane stress state is assumed, so the residual stress change is explained by the in-plane stress through the change in depth. The calibration constants can be obtained by numerical methods, because samples of any geometric shape can be studied, this method has high flexibility. The measurement procedure of incremental hole-drilling is very similar to the basic hole-drilling method, but it is divided into multiple drillings according to the predetermined depth of each drilling until the required drilling depth is reached, and recorded the strain that produced by each drilling and the actual diameter of the hole. then use appropriate calculation methods to get the magnitude of residual stress.

When measuring, according to the existing American standard ASTM: E837 recommended drilling method, the steps involved in the measurement are as follows:

- Install a special strain gauge rosette with at least three grids on the component to be analyzed for residual stress.
- Connect the rosette to a suitable instrument for recording strain.
- Adjust and set the drilling fixture.
- Establish zero depth, which is especially important for incremental drilling.
- Drilling in a series of depth increments to obtain data about stress changes with depth.
- Record the strain measured at each depth increment.
- Apply a series of equations to the measured value to calculate the residual stress state.

The following figure3 and 4 is show the styles of rosette most used in measurement. The size of the hole depends on the strain gauge used. The maximum depth of the hole is about 0.4D. Any larger depth is not necessary because the surface strain gauge is not sensitive for the depth increment beyond 0.4D. It is important to note that a highly accurate alignment and drilling system must be used for measurement.

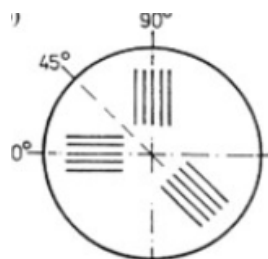


Figure 3. perpendicular rosette (0°/45°/90°)

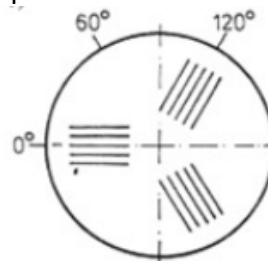


Figure 4. delta type rosette (0°/60°/120°)

In addition, it is better to drill with smaller depth increments under conditions, so it is recommended to use a high-speed air turbine for drilling. The system and equipment used to record the strain and hole depth measured at each increment is preferably automatic and can be electronically controlled. Take the MTS3000-Restan system currently on the market for measuring residual stress as an example. It is composed by a mechanical – optical fixture and an electronic device with a set of accessories and spare parts, in particular turbines and drills, connection

cables, set of tools, software protection key, dial gages, manometer and pressure regulator with air filter, manuals and software installation CD. The system permits to drill the material at 400,000 rpm: this avoid introducing any other residual stress into the material during the test process.

Figure 5 refers to a typical diagram from SINT Technology showing a measurement chain using a high-speed air turbine.

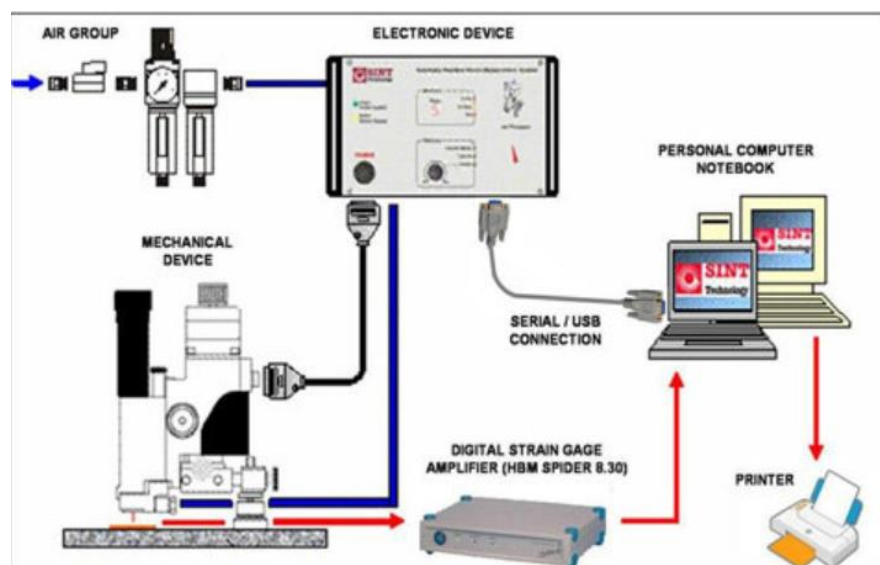


Figure 5. Diagram of the measurement chain using MTS3000-Restan

3.4.3 Apparatus preparation and technology

Strain measurement technology, drilling technology and analysis methods after the measurement are the main factors leading to deviations in results. When discussing measurement technology, the first thing to consider is the choice of strain gauge rosette. There are rosettes of various sizes and performances on the market, and many of them are specifically designed for drilling technology. All rosette designs include centering marks for accurate drill tool calibration. When selecting, the priority is its size, which depends on:

- Measure the size of the area.
- Predetermined depth required for residual stress analysis. The deeper the depth, the larger the required size.
- Acceptable damage to the component.

The most commonly used gauge size is an individual gauge with a length of 1.5mm. This gauge can provide useful residual stress data with a depth of about 1mm.

In addition to the size, when choosing the right strain gauge rosette, its availability and ease of handling are also very important.

The installation of the strain gauge rosette should follow the instructions of the strain gauge and adhesive manufacturer. The instructions provided by the UNI 10478 standard can also be referred to. The surface preparation and gauge installation process must be cautious, as this will directly affect the accuracy of strain measurement. The purpose of surface preparation is to make a surface suitable for bonding without changing the surface stress state. The surface preparation needs to remove oxides, rust, and paint on the surface. Since the incremental hole-drilling method is used to determine the stress, mechanical abrading should be avoided as much as possible.

Regarding adhesives, conventional cyanoacrylate adhesive is the fastest and most convenient choice for steel components.

The Figure below shows the previously mentioned MTS 3000-Restan, which is a typical alignment and air turbine drilling system. In this setup, the microscope is incorporated into the measurement system and will not be affected during the measurement.

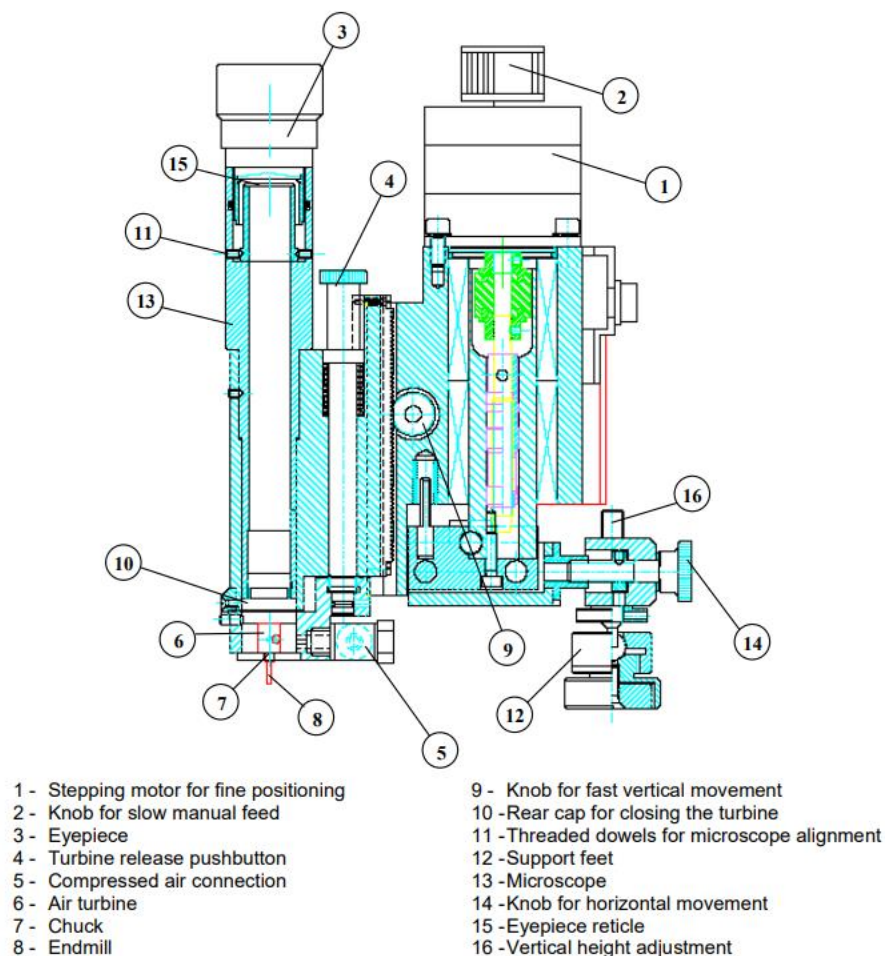


Figure 6. Hole drilling apparatus MTS 3000 - SINT Technology

ASTM E837 stipulates that the center of the hole should be concentrically aligned with the strain gauge circle and within $\pm 0.004 D$.

3.4.4 Drilling technology

Regarding the research of drilling technology, A.Ajovalasit, Bernardo Zuccarello, M.Beghini and Michele Scafidi(4) integrated five different drilling technologies in their report according to the research of M.T. Flaman and J.A.Herring (2, 3) , These technologies were compared based on the additional stress and geometry caused by different drilling methods and analyzed their portability and ease of use. The five drilling techniques are:

- high-speed drilling,
- low-speed drilling,
- abrasive jet machining,
- electro-chemical machining,
- high-speed orbital drilling.

High-speed orbital drilling is mainly used for high-hardness alloys. There is no need for reuse of steel structures, so the technical details will not be introduced in this section. The table provided below shows the geometric characteristics of the holes made by the first four drilling techniques. The table was researched and produced by M.T.Flaman.

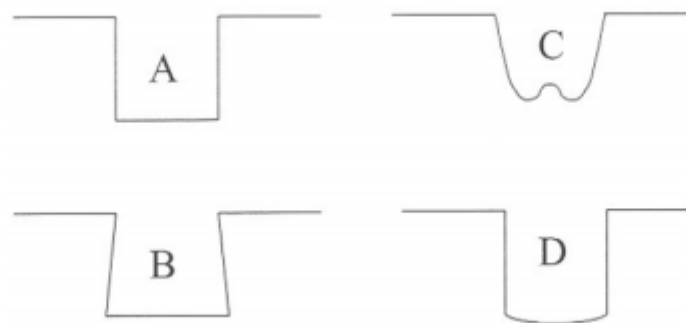


Figure 7. Geometry of the hole made from different technology by Flaman: A high-speed drilling; B low-speed drilling; C abrasive jet machining; D electro-chemical machining.

It can be seen from the table that among the first four drilling techniques, the geometry of the hole obtained by high-speed drilling is the most stable. Flaman used the air turbine drilling system when performing the high-speed drilling experiment. The rotation speeds up to 400,000 rpm, the typical equipment of this system has been mentioned in the previous section.

Low-speed drilling is the first drilling technique used to measure residual stress by the hole-drilling method. It has been widely adopted in the last century. However, Flaman's research shows that this technique will bring greater additional stress. Under the conditions, this technology is not considered for implementing the hole-drilling method.

It can be found from the geometry alone that abrasive jet machining is not suitable for hole-drilling method. As for electro-chemical machining, the geometry of the holes made by this technology is acceptable, but due to the problem of the chemical reagents used in the technology, it may have an adverse effect on the strain gauge grids. Due to these reasons, high-speed drilling is the most suitable technique which can be applied to the hole-drilling method.

3.4.5 Calculation methods

There is a method that can be used to calculate the residual stress in a homogeneous isotropic linear elastic material in the ASTM E837 standard in the United States. This method directly calculates the residual stress by using a specific rosette. To use this method to obtain accurate results, the measurement target needs to be in the following situations:

- the equ-biaxial component of the residual stresses is less than 50% of the yield stress.
- shear stresses in any direction are less than 25% of the yield stress.

However, for reused steel structures that have gone through the first life cycle, there are almost no components that meet the above conditions. Therefore, in this section, the method of calculating linear residual stress will not be introduced in detail. Compared with linear calculation, nonlinear residual stress calculation method is more suitable for reused structure.

Lars Fuglsang Andersen (5) gave two calculation methods for calculating residual stress through incremental hole-drilling method in his PHD thesis. Among them, it was mentioned that the integral method is very suitable for describing nonlinear variation in the stress field. Because of the above, the calculate steps and concepts of the integral method has been included in this section.

3.4.6 integral method

The development of the integration method began with the research of Bijak-Zochowski (6), and then gradually improved after the research of G.

S. Schajer (7, 8) and others. Figure 8 below depicts the state of the component when the method is applied.

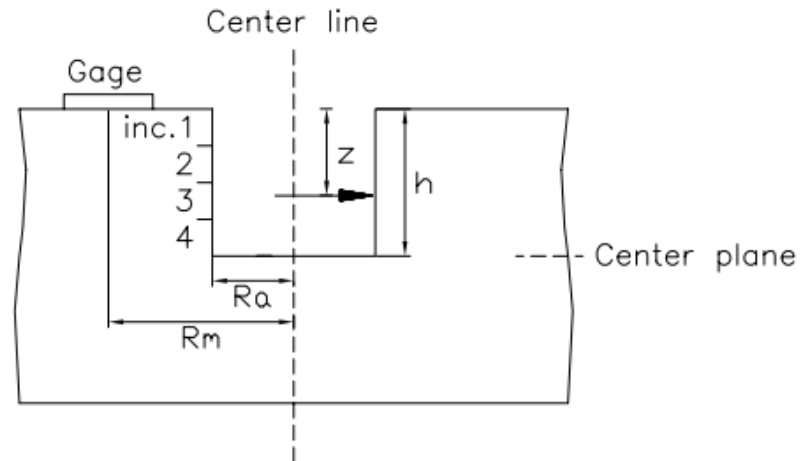


Figure 8. hole depth h and stress depth z

In the integral method, it takes into account the geometric effects caused by drilling. As shown in the figure above, when the drilling reaches the depth h , the residual stress released at each intermediate depth z between the surface and h will produce a measurable relaxed strain on the surface.

The relaxed strain generated by the residual stress released at z depends on the depth h , which is referred to as the geometric effect here.

This method needs to calculate the values of strain variables p , q , t at each hole depth, and the stress distribution can be obtained by solving the following three integral equations:

$$p(h_i) = \frac{1 + \nu}{E} \cdot \int_0^{h_i} \hat{A}(H, h_i) \cdot P(H) dH$$

$$q(h_i) = \frac{1}{E} \cdot \int_0^{h_i} \hat{B}(H, h_i) \cdot Q(H) dH$$

$$t(h_i) = \frac{1}{E} \cdot \int_0^{h_i} \hat{B}(H, h_i) \cdot T(H) dH$$

In these equations P , Q , T are combined stresses, corresponding to three sets of combined strains p , q , t . ν is Poisson's ratio, A and B are the influence coefficients on the hydrostatic stress state and the shear stress state, respectively. H is stress depth (same with z at Figure 8) and h is hole depth.

The influence coefficient is proposed by Schajer. In order to simplify the evaluation of residual stress, a certain coefficient can be considered to

determine the stress field at each depth. The coefficient has a fixed value, and it can be calculated for each step.

the equations shown above can be expressed in discrete form as:

$$\frac{E}{1+\nu} \cdot p_i = \sum_{j=1}^i \bar{a}_{i,j} P_j \quad E \cdot q_i = \sum_{j=1}^i \bar{b}_{i,j} Q_j \quad E \cdot t_i = \sum_{j=1}^i \bar{b}_{i,j} T_j$$

where n indicates the hole depth step considered, $\alpha_{i,j}$ and $b_{i,j}$ indicate the relieved strains due to unit stresses P, Q and T at depth j for hole depth step i .

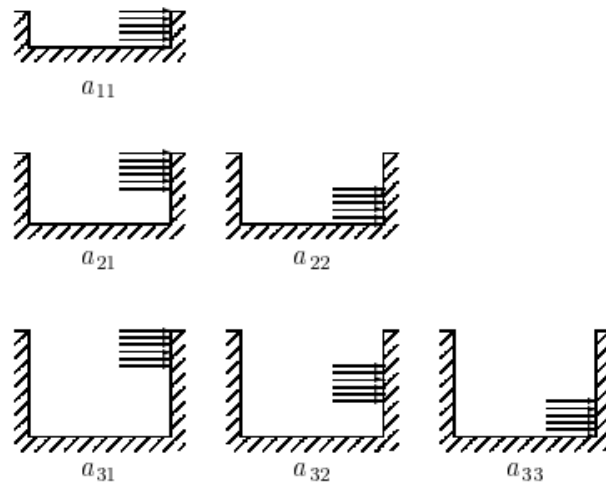


Figure 9. application of unit stress loads for derivation of $\alpha_{i,j}$

Through finite element calculation, the coefficients $\alpha_{i,j}$ can be calculated by the following functions.

$$\bar{A}(h, h) = \int_0^H \hat{A}(H, h_i) dH$$

$$\bar{a}_{i,j} = \bar{A}(H_j, h_i) - \bar{A}(H_{j-1}, h_i)$$

where A^\wedge is the influence functions for a hydrostatic stress state.

For each calculated increment, the residual stress, and the residual stress orientation (σ_{max} , σ_{min} , β) are obtained from the corresponding combined stresses.

$$\sigma_{min}(H) := P(H) - \sqrt{Q(H)^2 + T(H)^2}$$

$$\sigma_{max}(H) := P(H) + \sqrt{Q(H)^2 + T(H)^2}$$

$$\beta(H) := \frac{1}{2} \arctan\left(\frac{T(H)}{Q(H)}\right)$$

3.5 sectioning method to measure residual stress

The sectioning method is a method of measuring residual stress that has been used for more than one hundred years. This method has been proven to be effective, accurate and economical a long time ago. It is often used to measure the residual stress of steel components. Although it was proposed in the report of Ralakovsky (10) in 1888, it was not until 1972 that N. Tebedge, GA Alpsten and L. Tall (9) first tried to integrate the measurement procedure of the sectioning method into a standard measurement.

The principle of the sectioning method is to measure the variation of each strip and apply Hooke's Law, so that the stress distribution on the cross section can be determined reasonably and accurately. In the analysis, it is assumed that the transverse stress is negligible, but in fact the transverse stress may exist, but it will not produce obvious strain during the cutting process. This can simplify the analysis.

The residual stress distribution of the thickness of the plate can be determined by the variation of the strain readings after "slicing" sawing. The process of sectioning and "slicing" is shown in Figure 10.

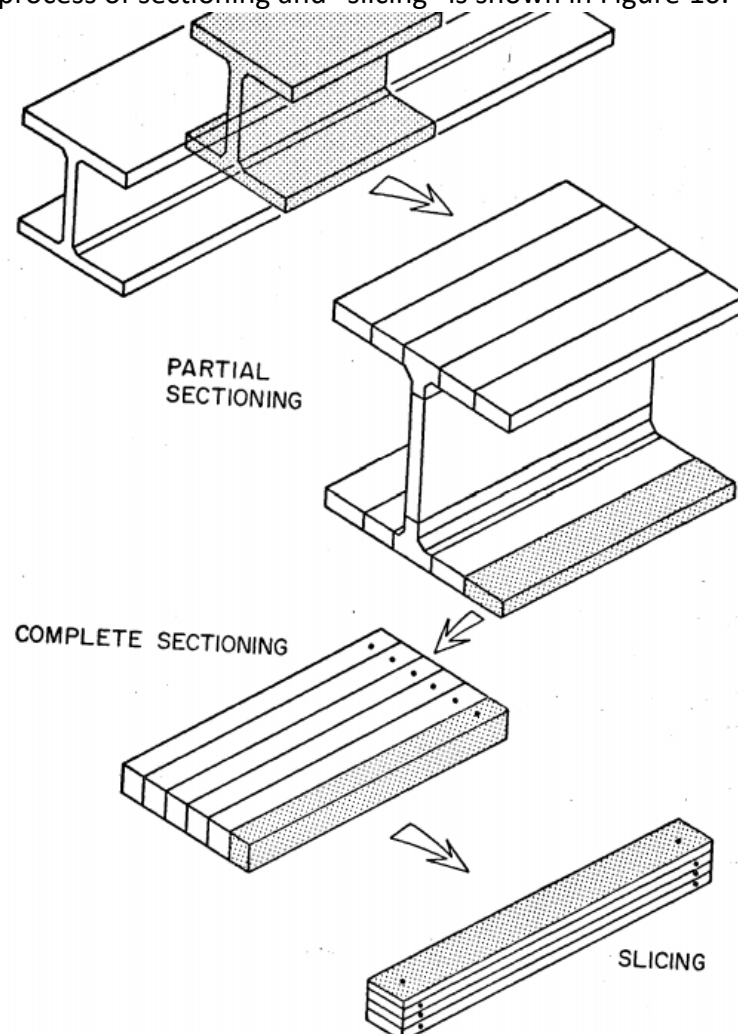


Figure 10. steps in the sectioning method

3.5.1 Sample preparation

The first step in preparing the sample is to cut the test member along the length of the material. In order to reduce the influence from the end, the intercepted test part must be far away from the end, and the recommended distance is 1.5 to 2 times the lateral dimension. Afterwards, the gauge hole must be prepared. The choice of the gauge hole size is related to the accuracy of the reading, so when preparing the gauge hole, it should be decided according to the choice of mechanical strain gauge.

The last is slicing, and the method of cutting can be partial sectioning. Before applying this method, it is necessary to estimate the distribution of residual stress and determine the number of longitudinal strips that need to be cut according to the steepness of the residual stress distribution gradient. The steeper, the smaller the spacing of longitudinal cutting. The cutting sequence has no effect on the final result because the unloading of the fiber is always in an elastic state.

3.5.2 Measurement

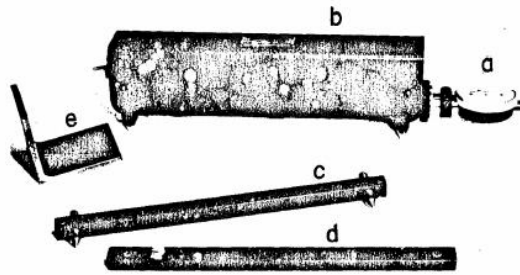
Since the mechanical extensometer is not attached to the specimen and is not easily damaged during the sectioning process, it can be repeatedly measured, so this equipment is widely regarded as suitable for the sectioning method. Whittemore strain gauge is a typical mechanical extensometer.

Whittemore strain gauge was invented by mechanical engineer Herbert L. Whittemore around 1926. It was usually used to measure the elongation of a 10-inch gauge in large structural parts (such as bridge trusses). As shown in Figure 11 below, it is an independent instrument consisting of two coaxial tubes, a pair of elastic hinges and a precise measuring tool. The instrument requires careful operation of the staff to avoid accidental longitudinal forces that applied by the operator.



Figure 11. Whittemore strain gauge

The following two pictures are schematic diagrams of whittemore strain gauges:



- a) Dial Indicator
- b) Body of Whittemore Extensometer
- c) Center Punch
- d) Reference Bar
- e) Positioning Angle

Figure 12. Composition of Whittemore strain gauge

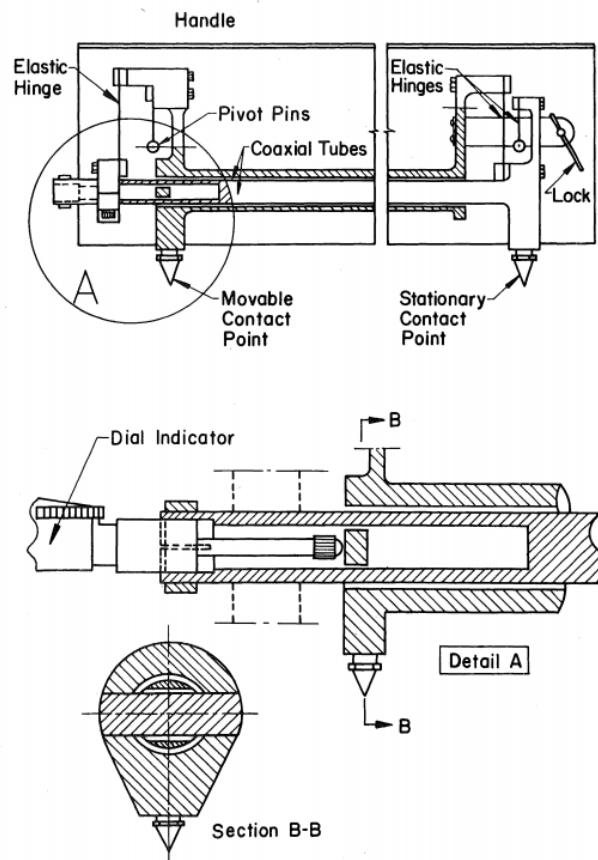


Figure 13. Schematic Diagram of the Whittemore Strain Gage

The main reason for the error in the measurement is probably due to temperature changes. Therefore, during the reading period, it is necessary

to place a reference bar of the same material as the test component on the tested component more than 1 hour in advance, and maintain a uniform temperature Measure under circumstances to ensure the accuracy of the experiment. The purpose of the reference bar is to eliminate errors caused by temperature changes.

The steel bar in the high stress gradient area (the area near the flame cutting or welding edge) will have obvious bending, and the change obtained by the extensometer is the change of the chord length, not the change of the arc length representing the actual strain. It must be given Certain correction: first measure the offset of the arc over the gage length on the bent steel bar, and then take the value and the change in chord length as the measured value, the true strain can be regarded as:

$$\bar{\epsilon} = \frac{\Delta L}{L} + \frac{(\delta/L)^2}{6(\delta/L)^4 + 1}$$

$\Delta L/L$ is the strain measured by the extensometer; δ/L is the ratio of the offset to the chord length.

3.5.3 Calculation steps

The calculated value is based on the assumption that the dimensional change caused by relaxation is a linear elastic change. The first step of the calculation is to calculate the average value of L read from each gage length:

$$L_{average} := \frac{\sum_{j=1}^n L_j}{n}$$

The average value is calculated for each reading interval, and then the strain caused by the relaxation caused by the slice and the strain caused by the temperature are calculated separately. The following is the strain caused by the relaxation:

$$\epsilon_o = \left[\frac{\bar{L}_i - \bar{L}_f}{\bar{L}} \right] \text{Specimen}$$

The strain caused by temperature is as follows:

$$\epsilon_T = \left[\frac{\bar{L}_i - \bar{L}_f}{\bar{L}} \right] \text{Ref. bar}$$

L_i and L_f are the initial measured gauge length and the final measured gauge length.

According to the above strain value, find the net value of residual strain caused by relaxation:

$$\epsilon_r = \epsilon_o - \epsilon_T$$

When there is obvious bending on the component, the following formula can be used instead to obtain a more accurate value:

$$\epsilon_r = \bar{\epsilon} - \epsilon_T$$

Finally, using Hooke's law to obtain the residual stress on the surface:

$$\sigma_r = - E \epsilon_r$$

4 LITERATURE REVIEW OF GEOMETRIC IMPERFECTION

4.1 Definition of geometric imperfection

Through the definition of geometric imperfection in "manual on stability of steel structures", the so-called geometric imperfection refer to the deviation of geometric form of the ideal structure and its components from the perspective of fabrication and erection and the need to achieve sufficient structural safety.

The geometric imperfection of the component directly affects the stability and bearing capacity of the component, so it needs to be taken seriously. As shown in the following Table 1, which is taken from EN 1993 1-5, the geometric imperfection of components is divided into local imperfection and global imperfection. Local imperfection refers to variation in the cross-section of components, which have a greater impact on the bearing capacity of thin-walled structures, and the cross-sectional geometry and distribution of such defects are more complex. The ordinary steel structure is mainly composed of non-thin-walled components, and the influence of section variation can be ignored, and the influence of the global geometric imperfection of the components is mainly considered. However, when measuring the geometric imperfections of the reused steel structure, the shape of components may change due to the residual stress generated in the first life cycle. Therefore, when talking about the reuse of the steel structure, the local imperfection cannot be ignored.

ECCS stipulates general tolerance requirements. The establishment of these requirements is based on the data collected by on-site measurement and the experience of many steel construction companies in European countries. Statistical analysis of these data is carried out. By assuming that the geometric imperfection can be measured by a normal distribution curve Characterization and can reasonably describe the allowable tolerance by using twice the standard deviation as the upper or lower limit.

In ECCS, the geometric imperfections used in the calculation of structural design will consider the following aspects:

- Product specification or execution standard to measure the local geometric tolerance of the produced product
- Structural imperfections due to fabrication and erection
- Residual Stress
- Changes in yield strength

According to the EN 1993 1-1 clause 5.3, the application of imperfections is organized into deflection and sway. Thus, imperfections could be considered by equivalent loads such as Figure 14.

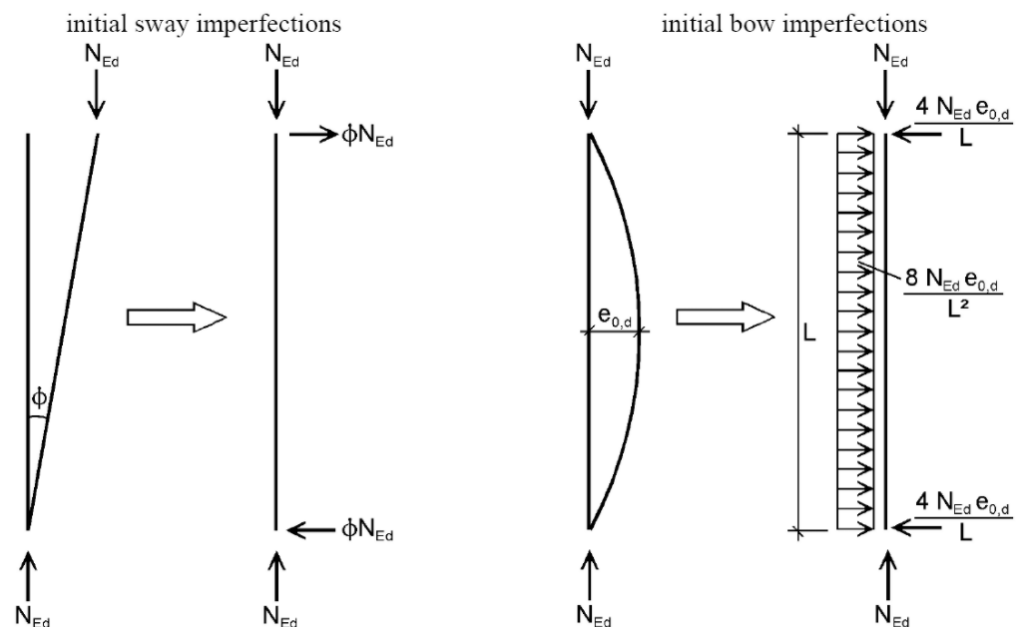


Figure 14. Equivalent loads according to EN 1993-1-1

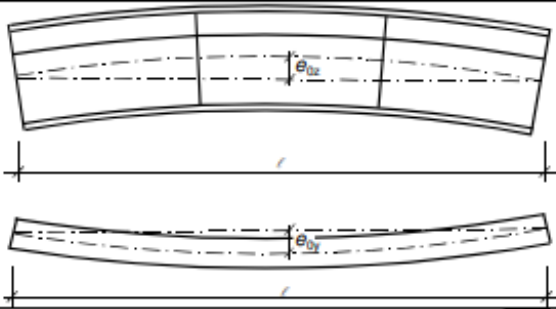
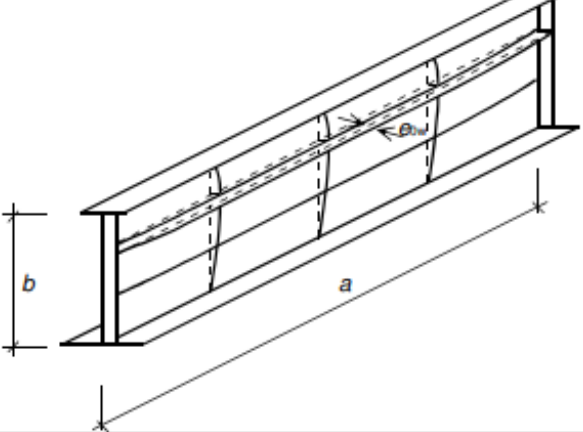
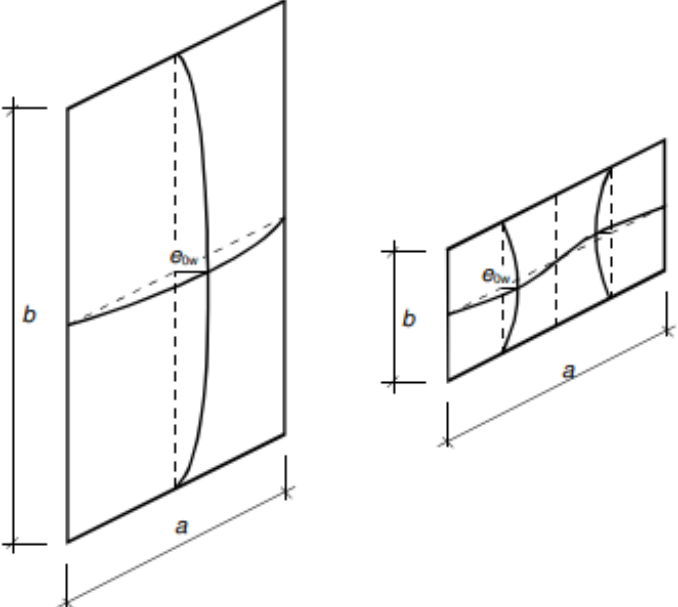
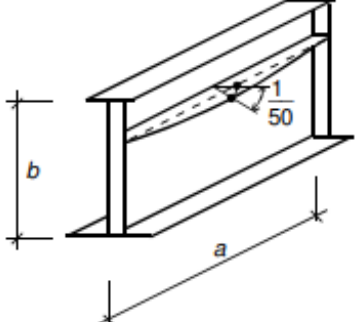
Type of imperfection	Component
global member with length ℓ	 <p>Two diagrams showing global imperfections in a member of length ℓ. The top diagram shows a curved member with a vertical imperfection e_{0z} at the center. The bottom diagram shows a curved member with a vertical imperfection e_{0y} at the center.</p>
global longitudinal stiffener with length a	 <p>A 3D perspective diagram of a global longitudinal stiffener with length a and height b. It shows a curved imperfection e_{0x} along the length of the stiffener.</p>
local panel or subpanel	 <p>Two diagrams showing local imperfections in a panel or subpanel with dimensions a and b. The left diagram shows a curved imperfection e_{0w} in a panel. The right diagram shows a curved imperfection e_{0w} in a subpanel.</p>
local stiffener or flange subject to twist	 <p>A 3D perspective diagram of a local stiffener or flange with length a and height b. It shows a twisted imperfection $\frac{1}{50}$ along the length of the stiffener.</p>

Table 1. local and global imperfection

4.2 The influence of geometric imperfection on steel structure

In reviewing the definition of geometric imperfections, according to ECCS, component geometric imperfections are divided into local imperfections and global imperfections, both of which have an impact on the performance of reused steel components. In this section, local imperfections, or variations of cross-section, will be explained and impact of variation on steel structures will be discussed.

4.2.1 hot-rolled steel structures

Before discussing the impact, the first thing is understanding how the cross-sectional variation occurs. The cross-sectional variation is caused by the irregularities of the cross-section and the unevenness of the cross-sectional elements. In the construction and production stage, when the components are rolled in the rolling mill, the shaping rollers will gradually wear, resulting in deviations in the cross-sectional dimensions of the rolled components. During welding, the thickness change of the rolled component plate and the height and width changes caused by manufacturing will cause the dimensional deviation of the welding shape. Next, the rolled plate will be an example to discuss the influence of the change in cross-sectional dimensions on the components.

The figure 15 below summarizes the dimensional changes of more than 5,000 H-beams rolled by a number of European steel mills, and finally included in the data analysis chart in "manual on stability of steel structures", mainly including light, medium and some relatively Heavy (flange thickness greater than 25mm) steel.

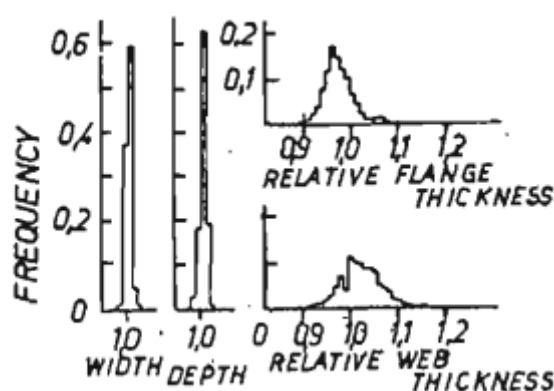


Figure 15. Dimensional variation of H-shape-steel

As can be seen from the figure 15, during the rolling process, the height and width changes are relatively small, while the thickness changes are large. Compared with the standard value, the thickness of the flange tends to become thinner, and the thickness of the web tends to become thicker.

The following Figure 16 is a graph of the changes in the geometric cross-sectional characteristics of H-shaped steel members obtained by sampling and surveying about 5,000 rolled H-shaped steel members of the same profile, including area A , moment of inertia I , section modulus W and the plastic section modulus Z .

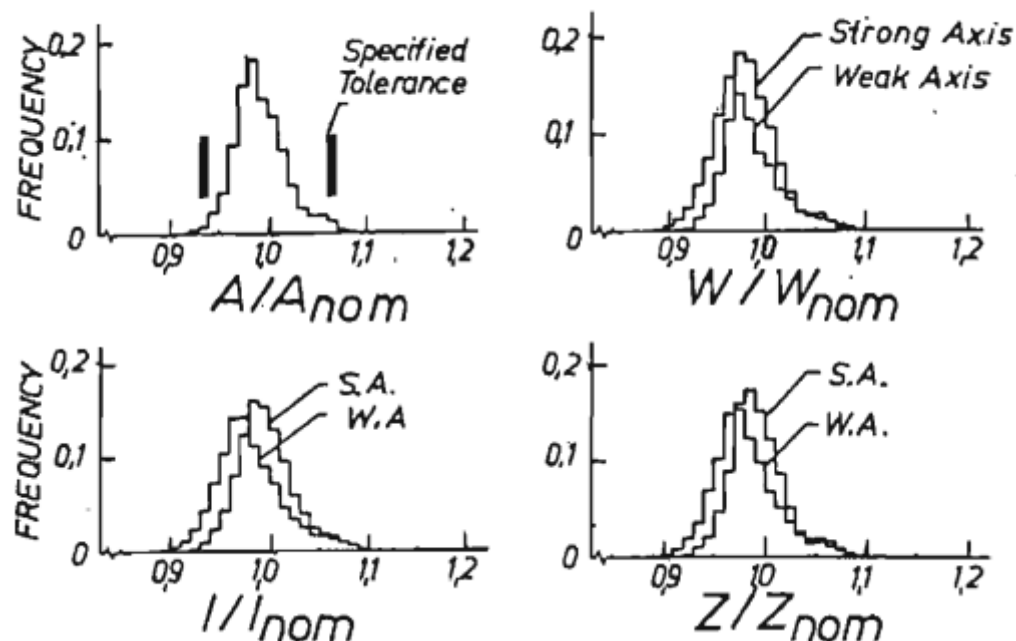


Figure 16. geometrical cross-sectional properties of H-shaped-steel

The curve distributions of the four cross-sectional characteristics shown in the figure above are very similar. Among them, the cross-sectional geometric characteristics of more than half of the components are lower than the standard value. Compared with the strong axis, the weak axis is much smaller than the standard value. Comparing Figure 16 and Figure 15, it can be found that the change in thickness seems to be the most important factor affecting the section characteristics.

According to the research results given by G.W.Schulz and G.Alpsten in <manual on stability of steel structures>(11), the influence of changes in cross-sectional properties on the ultimate strength of structural members is small and depends on the slenderness ratio under consideration. For small slenderness ratios ($\lambda \sim 60$), the effect of the change in cross-sectional area on the strength of the member, especially the yield strength is tiny, but for medium and high slenderness ratios, the effect of A change will be more obvious.

4.2.2 Cold-formed steel structures

The above introduced the influence of geometric imperfections on hot-rolled steel components, and the next thing to talk about is the influence of geometric imperfections on cold-formed steel components. Similarly, before introducing the influence of geometric imperfections, it is

necessary to understand the manufacturing process of cold-formed steel structures.

There are three main manufacturing processes on the market today: cold roll forming, pressure brake operation and bending brake operation. But for the cold-formed steel used in construction, most of them are produced by cold rolling. The process flow of cold rolling can be divided into the following five steps:

- 1 Raw steel are produced as the hot-rolled steel members.
- 2 Pour molten steel into the slab and form a thinner steel strip by rolling.
- 3 Zinc galvanizations is applied on thinner strips to form a steel coil.
- 4 Cut the large steel coil into a width that matches the required size.
- 5 At room temperature, use various rollers to form cold-formed steel components of the required shape.

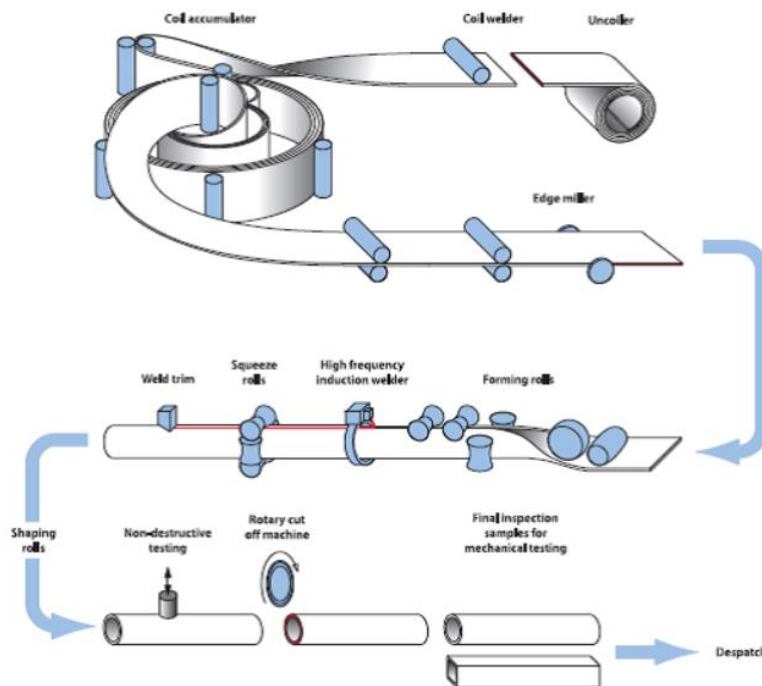


Figure 17. cold formed steel manufacturing process of tubular sections

Above figure from SteelConstruction.info that shows the Production process for structural hollow sections.

Various imperfections are caused during the manufacturing process, including geometric imperfections and residual stress. These imperfections are controlled within a certain range due to strict production standards, which mainly regulate regular shapes such as Z and C shapes. It has strict limits on dimensional deviations in production, but other

geometric imperfections such as distortion and bow imperfections will be generated during transportation and installation. According to Xi Zhao (12) on the sensitivity of cold-formed steel to geometric imperfections, consider the theory of buckling analysis, in practice, the column may be deformed by geometric deformation (i.e. initial imperfection) under a small load. Cold-formed steel is considered to be similar to the shape of the buckling mode, which will weaken the load-bearing capacity of the member.

Structural studs may yield or buckle. Short columns (small slenderness ratio) cause yield failure, while long columns (high slenderness rate) cause buckling failure, but medium-length columns are likely to be affected by geometric imperfections. Xi Zhao conducted simulation experiments based on the above viewpoints, and finally concluded that the structural member may fail earlier due to buckling instead of yielding at a smaller slenderness ratio.

4.3 Geometric imperfection measurement

The measurement of geometric imperfection is divided into the measurement of global imperfections and the measurement of local imperfections. This section will introduce two simple and feasible measurement method based on CN103968793 of imperfection measurement.

4.3.1 Measurement method of initial local geometric imperfections

This is a method of measuring the initial geometric imperfections of multiple measurement sections of steel members by using a resistive displacement transducer and a steel ruler. This method is selected because of its convenience, low equipment requirements, and high effectiveness and reliability. It from Document CN103968793A of Hefei University of Technology.

Refer to Figure 18, the measurement method of initial geometric imperfections of steel members is as follows:

First fix the component on the horizontal platform, fix a horizontally placed steel ruler on one side of the component parallel to the measuring section, and then fix the magnetic support of the resistive displacement transducer close to the side of the steel ruler that close to the component, At the same time, let the front-end probe of the resistive displacement transducer hang above the outer edge of the component that away from the steel ruler, but do not touch the measurement surface of the component, and record the initial position of the magnetic support of the resistive displacement transducer aligned with the steel ruler.

Then connect the data acquisition instrument with the resistive displacement transducer and clear the initial data on the data acquisition instrument. Adjust the position of the resistive displacement transducer so that it is perpendicular to the measuring surface of the component and make its front-end probe contact with the measuring surface of the component and gradually press it down. The real-time reading of the data acquisition instrument ensures that the length of the probe is just the half of the maximum range, the purpose of this is to allow the front-end probe in the measurement process to be extended or shortened, and the distance is half of the maximum range, to ensure effective measurement of large initial local geometric imperfections.

The third step is to fix the resistive displacement transducer on the magnetic support, clean up the data of the collector again, then loosen the magnetic support, move a certain distance along the steel ruler toward the principle component, and fixed the magnetic support again, and new data is recorded by the data acquisition instrument. The cycle repeats. Each time the magnetic support moves the same distance, the data is read once, until the front-end probe of the resistive displacement transducer moves to the component measurement section close to the outer edge of the steel component. Then put the magnetic support of the resistive displacement transducer back to the original position of the steel ruler, loosen the component and reverse the component, repeat the above steps to measure the initial local geometric imperfections on the other side surface. Until all surfaces are measured completion, all initial local geometric imperfections are obtained.

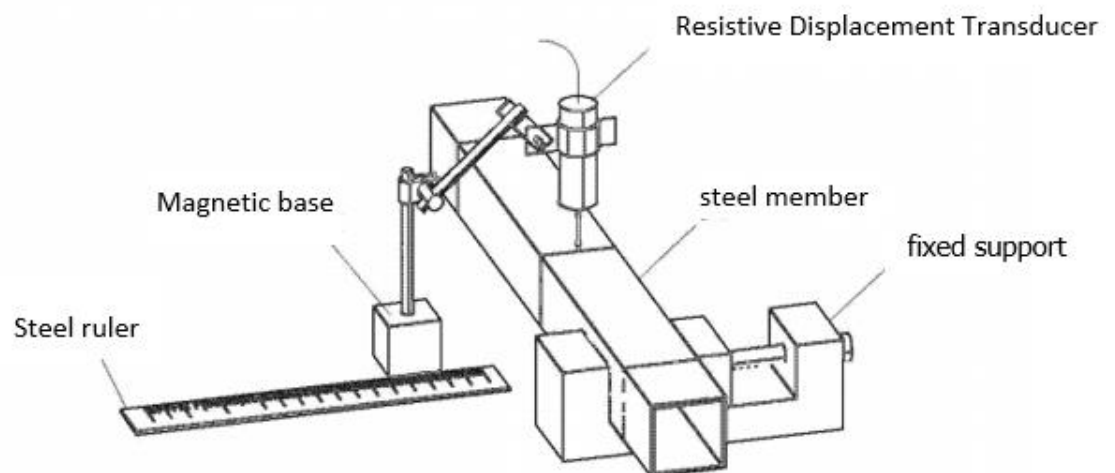


Figure 18. Schematic diagram of local imperfection measurement

When using this method, pay attention to keeping the distance between the steel ruler and the edge of the component moderate, not too close or too far, too close or too far will reduce the measurement range of the resistive displacement transducer.

When performing the third step, the distance of each movement of the magnetic support is determined by the cross-sectional size of the component and the accuracy requirements of the measurement. If it is required by higher accuracy, the distance of each movement can be slightly smaller, so that the measurement point of the measurement become denser, the data obtained will be more accurate.

If the funds are sufficient, a three-dimensional coordinate measuring instrument can be used when using this method, which can make the measurement accuracy reach 0.001 mm and realize the full automation of the measurement process.

4.3.2 Measurement method of initial global geometric imperfections

This section will introduce a measurement method seen from the document CN103968814B of Hefei University of Technology that uses an optical theodolite and an ordinary steel ruler to measure the initial imperfections in different areas of a metal component, and then uses a formula to calculate the initial global geometric imperfections of the component according to the geometric relationship of the measurement area.

As shown in Figure 19, the following is the specific content of the method:

First of all, prepare an instrument that can fix the components. In CN103968814B, the Universal testing machine is selected for the fixation of the components, then place the instrument on the test point. Although the document clearly states that the Universal testing machine needs to be used, since its purpose is only to fix components, other equipment that can fix components can also be applied. Next is place a tripod at a certain distance from the test point. Place the optical theodolite horizontally on the tripod and fix it. Adjust the height of the tripod so that Keep the theodolite parallel to the ground. Then place the component to be measured vertically on the test point of the universal testing machine, fix the horizontal axis of the theodolite, and observe the vertical lines at the top and bottom of the component by moving the theodolite's mirror tube on the vertical plane to ensure that the component remains vertical to the ground.

then apply a small load to the component through the universal testing machine to make the component fixed, after that loosen the horizontal axis of the theodolite, align the lens barrel to the right side of the component, and keep the track in a straight line when moving the lens barrel up and down on the vertical plane. Make sure that the straight line is always on the outer edge of the right side of the component and keep a distance from the outer edge. Fix the horizontal axis of the theodolite again, Place a steel ruler on the top, middle and bottom of the right section

of the component respectively, and move the lens barrel vertically to read the intersection of the lens tube and the steel ruler at the top, middle and bottom of the member respectively. The reading at the top is a_1 , the middle is b_1 , and the bottom is c_1 . a_1, b_1, c_1 , can calculate the initial global geometric imperfections of the section on the right side of the component according to a certain geometric relationship:

$$\delta_1 = |b_1 - c_1| - \frac{|a_1 - c_1|}{2}$$

Then select different positions of the top, middle and bottom of the right side of the component to place the steel ruler, repeat the above steps to read the different sets of readings $a_2, b_2, c_2, a_3, b_3, c_3, \dots$, and then calculate the different imperfection values, take the largest value is used as the final global imperfection of the right plane.

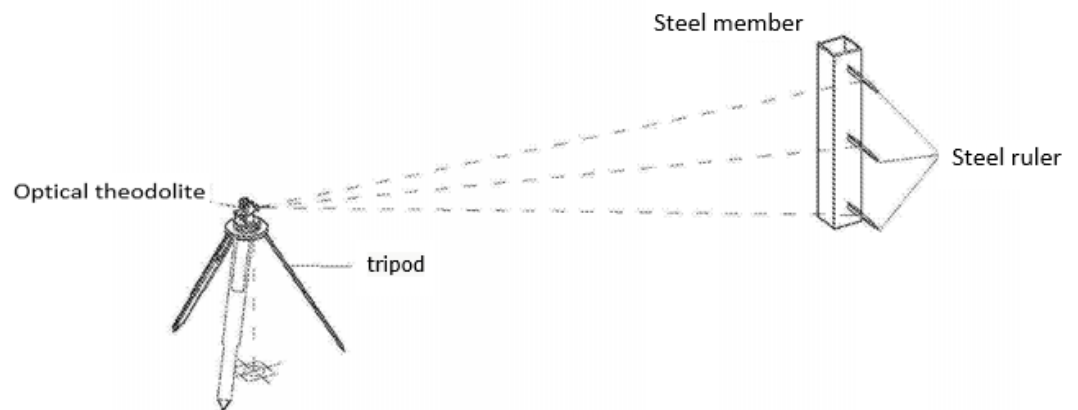


Figure 19. Schematic diagram of global imperfection measurement

When using this method, the load applied to the component by the universal testing machine must be appropriate, and the component must be in a completely elastic state, so that the load will not affect the measurement of the initial global geometric imperfection of the component.

4.4 Geometric imperfection measurement of cold-formed steel

The above-mentioned geometric imperfection measurement method is suitable for measuring hot-rolled steel structures, but it is difficult to ensure accuracy for cold-formed steel structures. Therefore, this section will introduce a laser-based method for measuring the geometric imperfection of cold-formed steel structures.

In 1886, Ayrton and Perry (16) published a paper on pillar buckling. They pointed out in the paper that the actual buckling load capacity of the

"stocky" column is much lower than the theoretical "crush" load. According to Euler's formula, it is generally believed that the "crush" load is greater than the buckling load. The key factor that makes this result is geometric imperfection. From this moment on, people have realized the importance of geometric imperfection.

The method to be introduced in this section was designed by M. Tootkaboni, B.W. Schafer and X.Zhao (13). It uses laser triangulation technology to measure imperfections through scan along the target cold-formed steel components. Scanning produces a large number of measurement point clouds, which can further explore the influence of geometric imperfections, especially for the influence of cross-sectional imperfections that are difficult to measure in the past limited by measurement methods.

Figure 20 shows the overview of equipment. The whole set of equipment is composed of laser scanner, rotating platform, triangular support frame and linear motion system. The purpose of designing this equipment is to accurately measure the geometric imperfections of cold-formed steel. Therefore, a laser-based measurement system is selected, which can provide accurate Data, and due to the large size of the object to be measured, the laser sensor will be placed on a movable platform.

The laser scanner is a 2D line laser, each reading can produce 800 points, and the maximum coverage width is 240 mm. It is located on a rotating table with a diameter of 635 mm. This allows the laser scanner to scan different parts of the target sample. The support frame equipped with the rotating table is heavy and wide enough to carry the rotating ring without tipping over, and only produce a small force on the linear guide. Placing the sample on the support beam can minimize deflection under gravity load. The linear motion system positions the laser along the length, so that the global geometric information of the target sample can be obtained by scanning the sample from multiple angles and recording each scan in the same final global coordinate system.

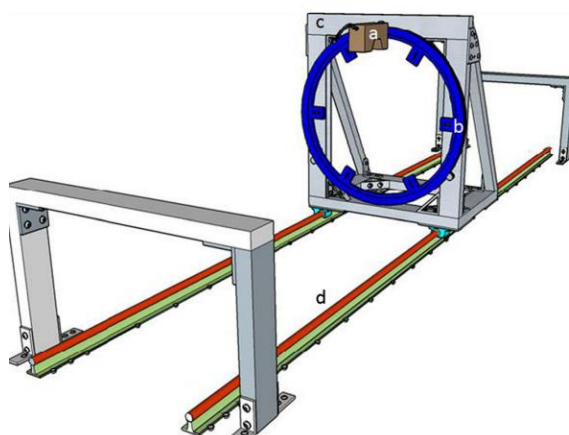


Figure 20. Equipment overview

As shown in Figure 21, the rotating platform, as other wards, is a rotary stage system, which is designed to rotate the laser head to any desired angle. The system consists of the following components: a large diameter rotary ring, a timing belt fixed on the rotating ring, and a stepping motor (Long Motor 23HS9430).

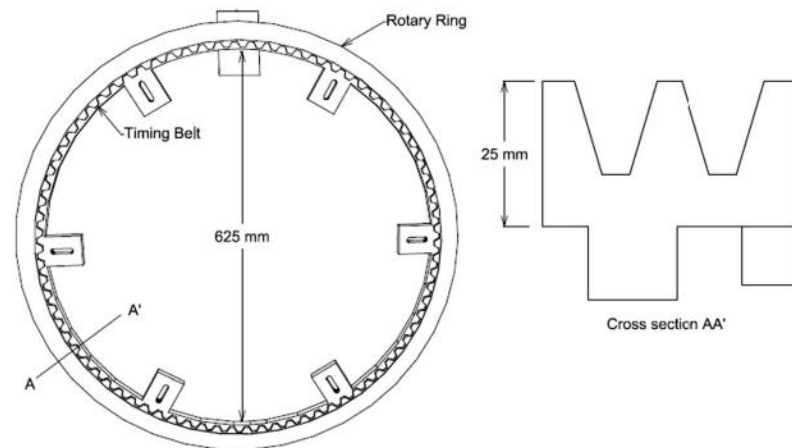


Figure 21. steel ring

The triangular support frame is used to fix the rotary platform and is driven by the linear motion system. The triangular design of the support frame can prevent the rotary platform and its heavy rotary ring from tipping over as shown in Figure 22. The triangular frame effectively distributes the load to the guide rails and provides stable movement of the laser and rotating system.

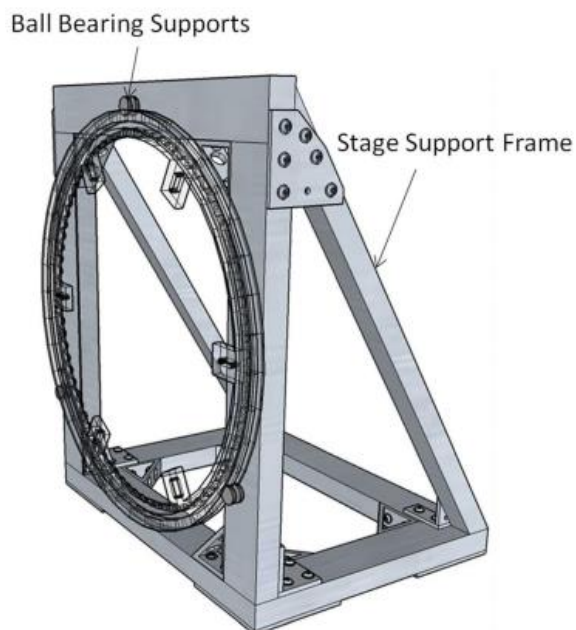


Figure 22. detail of triangular support frame

The linear platform system can be divided into the following two parts: the motion system and the linear guide system. Figure 23 depicts a general diagram of its operation. The linear motion system has an encoder at both ends, numbered 1, and the two are connected. Encoder 2 is embedded in the motor (GM9236S019) system. Connect the motor, drive chain and sprocket, and encoder 1 (ENS1J-B28) through a shaft coupling.

The function of encoder 1 is to control the motor, and the signal of encoder 2 (HEDS-91X0) is used to trigger the laser scanner. The linear guide system consists of double guide rails and four ball bearing supports, the purpose is to provide smooth movement. The triangular support frame is located on the four ball bearing supports. When the heavy equipment moves along the rail, the four ball bearing supports can automatically adjust the movement deviation.

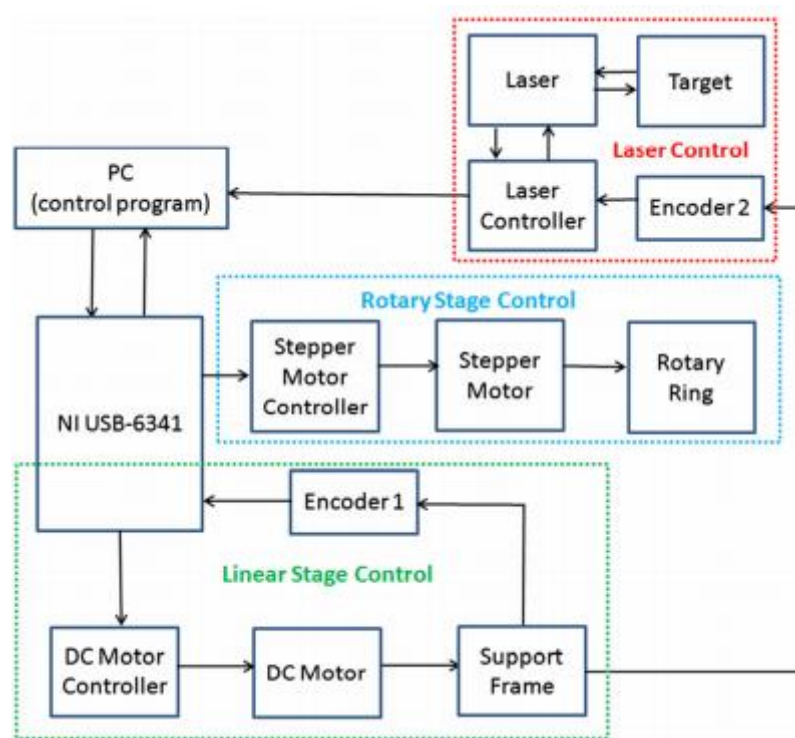


Figure 23. Automation of measurement platform through LabVIEW program

The linear position of the laser system is determined by two encoders, which are connected to the drive shaft of the linear motion system. As mentioned above, the encoder 1 provides the main longitudinal measurement for the linear motion system. Calibrate by using calliper and dial indicator measurement standards to convert the rotation count on the encoder into a displacement along the linear guide, and the result will be used as a linear calibration coefficient for the measurement platform.

The encoder 2 is used to trigger the laser, and even if the scanning speed changes, it can be measured at discrete intervals along the length. In addition, the encoder 2 also provides longitudinal laser position measurement through calibration. Calibrate by using a calliper measurement standard to convert the rotation count on the encoder into a displacement along the linear guide. As with encoder 1, the result obtained is used as a linear calibration coefficient for subsequent measurements.

Regarding the calibration of the rotary table, a simple inclinometer directly clamped on the laser head bracket will be used to calibrate the stepping motor that provides the rotation of the rotary ring. The accuracy of the inclinometer is 0.01° . The linear calibration coefficient is established through a series of rotating experiments, and then used for the control of the rotary ring.

Because each trigger scan of the line laser provides 800 readings in the local coordinate system d ($d = 300$ mm) from the laser head, it is necessary to convert the local coordinate system to the global coordinate system to combine multiple readings to present a complete scan result. To this end, Xi Zhao provides a new coordinate system and notation as shown in Figure 24 for the basic conversion from local coordinates to global coordinates.

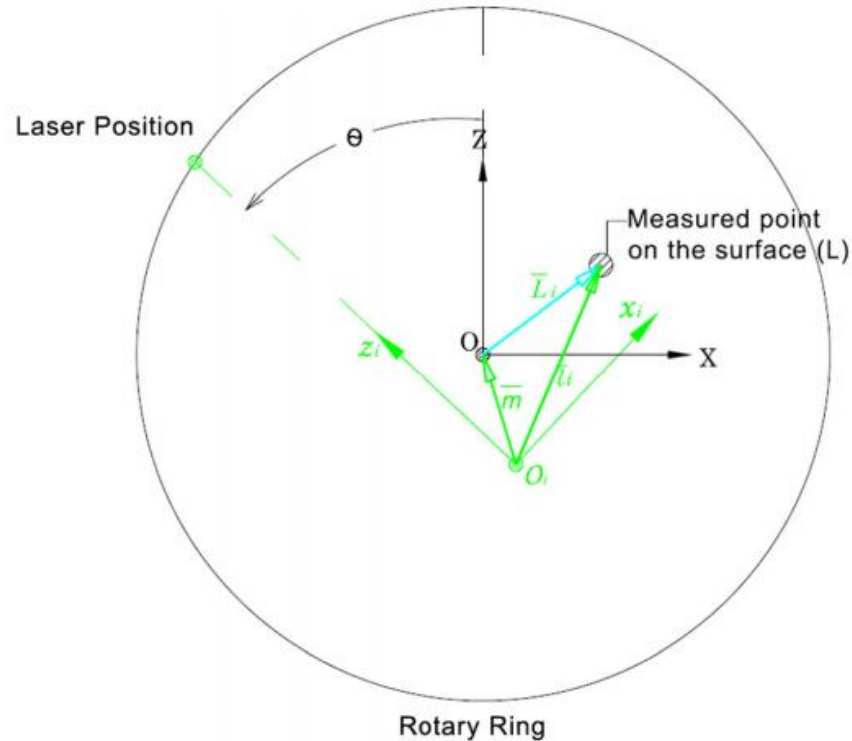


Figure 24. Global coordinates L_i and laser local coordinates l_i

A laser reading in the global coordinate system can be calculated from this formula:

$$\bar{L}_i = T_i (\bar{l}_i - \bar{m})$$

$$\text{where } T_i = \begin{bmatrix} \cos(\theta_i) & \sin(\theta_i) \\ -\sin(\theta_i) & \cos(\theta_i) \end{bmatrix}$$

To ensure the validity of the above formula, Xi Zhao tested the feasibility of the formula by using the statistical hypothesis of analysis of variance (ANOVA). In terms of the result, the deviation of the rotation center was very small, and the formula was satisfactory.

5 FINITE ELEMENT METHOD

The finite element method is the one of the most significant achievements in the field of computational methods in the last century. It originated from the analysis of aerospace structures. These frame structures are regarded as a combination of one-dimensional components. For these components, the exact solution of the differential equation for each component was well known. These solutions were cast in the form of a matrix relationship between the force and displacement at both ends of the component. Therefore, this method was originally called the matrix analysis of the structure. Later, it was expanded to include analysis of the continuum structure. Because the continuum structure has a complex geometry, it must be subdivided into simple components or "elements" interconnected at nodes. It was at this stage of method development that the term "finite element" emerged.

Nowadays, in the design of steel structures, it was common to use the finite element method to analyse more complex structures. For the reused steel structures, it was necessary to use the finite element method to simulate and analyse the geometric deformation and stress.

In fact, thanks to the development of computer technology, there are many commercial finite element software in the world today, which can simulate linear and nonlinear, whether it is material or geometric shape, metal forming, temperature, etc... At the same time, they also have advanced pre-processing and post-processing functions. This chapter will introduce a commercial finite element software called ABAQUS, which has been widely used in the field of civil engineering research, such as the

study of mechanical properties of building structures under static load, reciprocating load, impact load and fire.

5.1 Introduction of the ABAQUS

ABAQUS is a powerful finite element software for engineering simulation, which can solve problems ranging from simple linear analysis to many complex nonlinear problems. ABAQUS includes a rich cell library that can simulate any geometric shape. It also has various types of material model libraries, which can simulate the performance of typical engineering materials, including metals, rubber, composite materials, reinforced concrete, compressible super-elastic foam materials, and geological materials such as soil and rock as general simulation tools. In addition to solving a large number of structural (stress/displacement) problems, ABAQUS can also simulate many problems in other engineering fields, such as heat conduction, mass diffusion, thermoelectric coupling analysis, acoustic analysis, and rock and soil mechanics analysis.

This software is also widely regarded as the most powerful finite element software, which can analyse complex solid mechanics and structural mechanics systems, especially capable of handling very large and complex problems and simulating highly nonlinear problems. ABAQUS can not only analyse the mechanics and Multiphysics of a single part, but also perform system-level analysis and research. The characteristics of ABAQUS's system-level analysis are unique compared to other analysis software. Because of its excellent analytical capabilities and the reliability of simulating complex systems, ABAQUS has been widely used in industries and research in various countries.

5.1.1 Finite element analysis process by ABAQUS

In ABAQUS, the finite element analysis process can be divided into the three following stages:

Modelling stage: The modelling stage is to establish a finite element analysis calculation model based on the actual shape of the structure and actual working conditions, to provide the necessary input data for finite element numerical calculation. The central task of finite element modelling is structural discretization, that is meshing. But still have to deal with a lot of work related to it: such as structural form processing, collection model establishment, unit characteristic definition, unit quality check, number sequence and definition of model boundary conditions, etc.

Calculation stage: The task is to complete the numerical calculation related to the finite element method. Due to the large amount of calculation in this step, this part of the work is controlled by the finite element analysis software and completed automatically on the computer.

Post-processing stage: Its task is to perform the necessary processing on the calculated output results and display them in a certain way, so as to evaluate the structural performance or the rationality of the design, and make corresponding improvements or optimizations.

5.1.2 Commonly used function modules in ABAQUS

The following functional modules are often used during the entire operation of ABAQUS for finite element analysis of structures including steel structures:

Part: In the Part module, the user can generate a single part by operation, or directly use the graphics tool to generate the geometric shape of the part in the ABAQUS/CAE environment, or input the part from other graphics software.

Property: In the Property module, users create section and material definitions and assign them to components. The definition of the section includes part characteristics or part area information, such as the area's related material definition and cross-sectional shape information.

Assembly: The user can use the Assembly module to generate a copy of the part and position the copy of each part in the overall coordinates to generate an assembly. An ABAQUS model contains only one assembly.

Step: The user uses the Step module to generate and configure analysis steps and corresponding output requirements. The sequence of analysis steps provides a convenient way to reflect changes in the model (such as changes in loads and boundary conditions). Between steps, output requirements can change.

Interaction: In the module, the user can specify the mechanical and thermal interactions between various regions of the model or between a region of the model and the environment, such as the contact relationship between two surfaces. If the contact relationship is not specified in the Interaction module, ABAQUS will not automatically identify the mechanical contact relationship between component copies or between various areas of an assembly.

Load: Load, boundary conditions and fields can be specified in the Load module.

Mesh: The Mesh module contains various levels of automatic generation and control tools for finite element meshes.

Job: Once the model is completed, the user can use the Job module to implement analysis and calculations.

Visualization: The visualization module provides graphics of the finite element model and analysis results. It obtains model and result information from the output data, and the user can modify the output requirements through the Step module to control the storage information of the output file.

Sketch: The Sketch module can be used to directly generate plane parts, generate beams or a sub-area, or generate two-dimensional contour lines, and then generate three-dimensional parts by stretching, sweeping, and rotating. In ABAQUS, drawing a two-dimensional contour line first helps to generate the shape of the part.

5.2 Assign imperfection and residual stress to model

When using the finite element software ABAQUS, there are usually two methods to view the effects of residual stress and geometric imperfections on steel components. The first method is to Import the residual stress data and geometric imperfection data of the component into the model created by ABAQUS when these data are known. and then conduct force analysis to get the influence of residual stress and geometric imperfections on it. The second method is to simulate the effect of the thermal reaction on the component during welding or cutting, and to check the residual stress and geometric deformation in the component after the welding or cutting is completed and cooled.

It should be noted that the second method is difficult to simulate and the accuracy of the data obtained fluctuates greatly. Therefore, the first method that can be analysed by importing accurate data is more popular than the second method.

Regarding how to import geometric imperfections, the most used method is to find the .inp file of the existing model in ABAQUS and modify the node data in this file to realize the import of geometric imperfections. Specific steps are as follows:

- Prepare the .inp file of the existing model, find the *node part in it and copy it to the Excel.

- Prepare the existing position coordinates for each node (refer to the coordinate system in ABAQUS).

-Manually modify the coordinates of each node in the Excel.

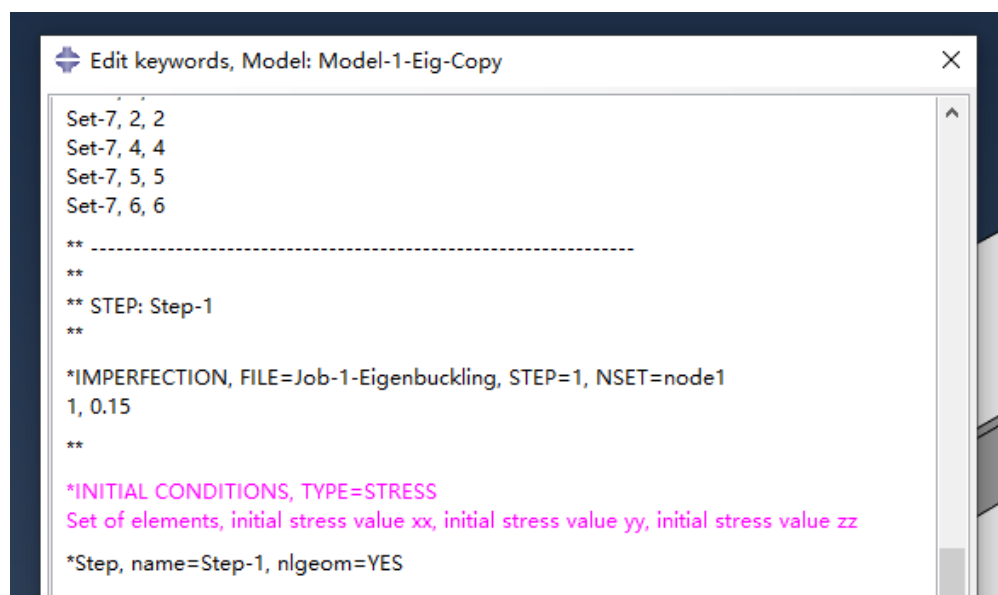
-Copy this updated *node segment to modify the original .inp file.

The above are the steps on how to import geometric defects, and for residual stress, it is imported by way of keyword modification. Proceed as follows:

-Define the element set of the assembly.

-Create the local coordinate of the element.

-As shown in Figure 25, open the instruction box by editing keywords and enter the text in the figure.



```

Edit keywords, Model: Model-1-Eig-Copy
Set-7, 2, 2
Set-7, 4, 4
Set-7, 5, 5
Set-7, 6, 6
** -----
**
** STEP: Step-1
**
*IMPERFECTION, FILE=Job-1-Eigenbuckling, STEP=1, NSET=node1
1, 0.15
**
*INITIAL CONDITIONS, TYPE=STRESS
Set of elements, initial stress value xx, initial stress value yy, initial stress value zz
*Step, name=Step-1, nlgeom=YES

```

Figure 25. the instruction box of keywords

The next section will show how to introduce initial imperfections in ABAQUS and the effect of imperfections on steel components through a buckling analysis of a simple beam model.

5.3 beam buckling analysis

5.3.1 Purpose

The overall instability of components caused by axial stress has always been a prominent problem in the research of steel structures. The main factors leading to this problem are the longitudinal residual stress on the component, initial geometric imperfections, and poor end restraints. As for the reused steel structures, the residual stress and geometric imperfections carried by steel components will undoubtedly increase after a series of disassembly and assembly. Therefore, a simple beam model was

established to predict that how the growth of imperfections will affect the stability of steel components.

5.3.2 Profile, loading, boundary condition of the component and research method

The 3000mm IPE300 with strength of S355 was used in this example, and all material properties are taken according to Eurocode. As shown in the figure 26, the steel beam constrained by a hinged support at both ends was subjected to longitudinal concentrated forces at 800mm and 2200mm. In order to avoid the occurrence of torsion, the force applied in this example would acts through shear center.

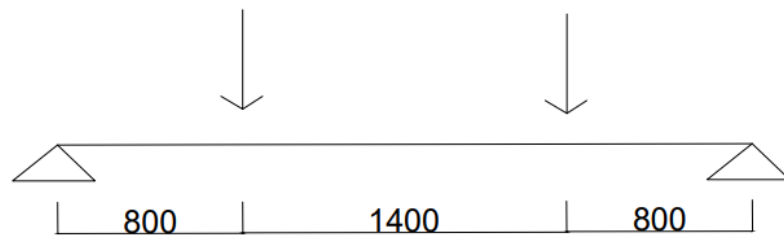


Figure 26. loading and boundary condition

In this case, nonlinear post-buckling analysis including geometric nonlinearity, material nonlinearity and residual stress will be used to study the stability of steel members under different imperfections.

Material nonlinearity will include by using stress-strain curve.

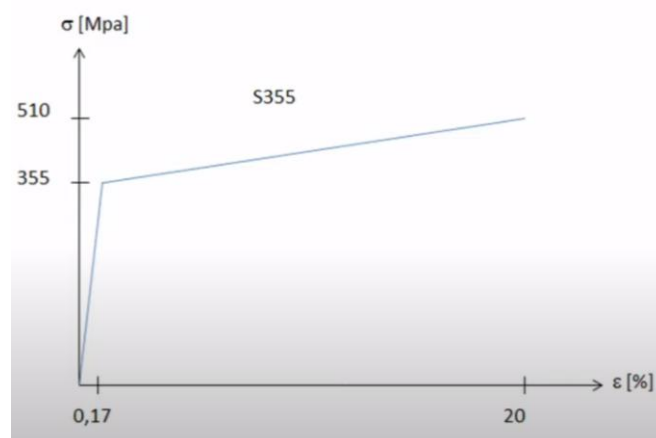


Figure 27. S355 stress-strain curve

According to EUROCODE, by using equivalent geometric defects, geometric nonlinearities and residual stresses can be included, which means that defects larger than actual conditions will be used in the model

to replace residual stresses and geometric nonlinearities, such as initial bow.

Buckling curve acc. to Table 6.1	elastic analysis	plastic analysis
	e_0 / L	e_0 / L
a ₀	1 / 350	1 / 300
a	1 / 300	1 / 250
b	1 / 250	1 / 200
c	1 / 200	1 / 150
d	1 / 150	1 / 100

Table 2. Design values of initial imperfection

5.3.3 Process

The main steps of nonlinear post-buckling analysis in ABAQUS can be simply divided into three steps: Eigenvalue buckling analysis->Generate initial imperfection file->Perform nonlinear full-process analysis.

at the first, eigenvalue buckling analysis should be performed. This analysis is linear buckling analysis, which is carried out under the condition of small deformation, that is, elastic buckling mode. The purpose is to generate the critical value (take the eigenvalue of the first-order buckling mode multiplied by the set value), and output the corresponding predetermined displacement set. To perform Eigenvalue buckling analysis, first draw the section of the component at the function-part as the Figure 28.

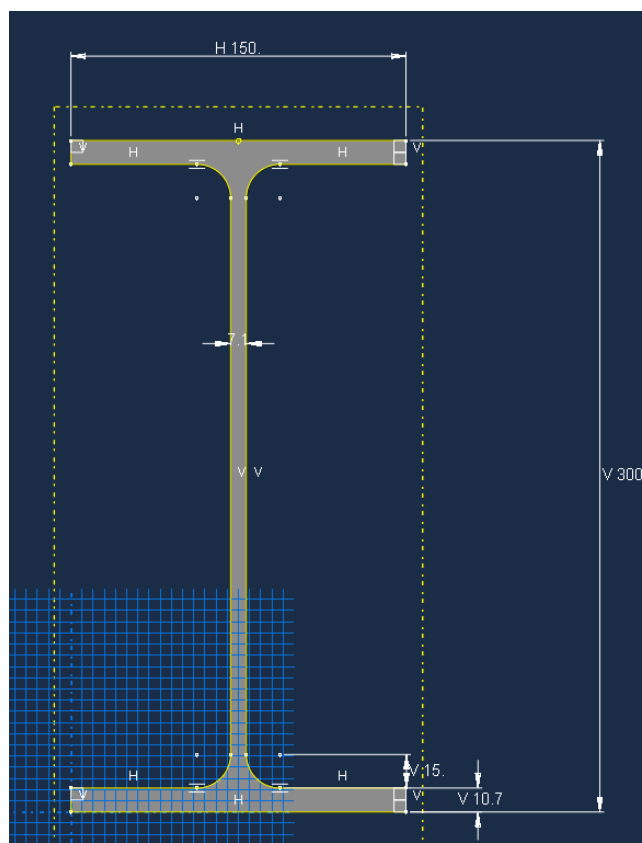


Figure 28. Section of IPE300

Then create the material properties of the steel member in the function-property, only the elastic analysis would be used when performing Eigenvalue buckling analysis. Therefore, define the Young's modulus as 210000MPa and the Poisson's ratio as 0.3. The material properties are matched with the previously established section. Create instance in function-assembly

in function-step, select linear perturbation for procedure type, and then select buckle. Eigensolver and number of eigenvalues are shown in Figure 29.

Type: Buckle

Basic Other

Description:

Nlgeom: Off

Eigensolver: Lanczos Subspace

Number of eigenvalues requested:

Maximum eigenvalue of interest:

Vectors used per iteration:

Maximum number of iterations:

Figure 29. Edit of step

Create two concentrated forces and constraints as shown in Figure 26 at function-load. For the value of the concentrated force, the unit load should be used.

The next step is to divide the mesh for the component. Because the student license can only create a mesh below 1000 nodes, it is impossible to choose a particularly accurate mesh. The mesh is shown in the figure 30. Then copy the model in the model tree. The purpose of this is to obtain a model that has the same mesh and can import initial imperfection during nonlinear full-process analysis.

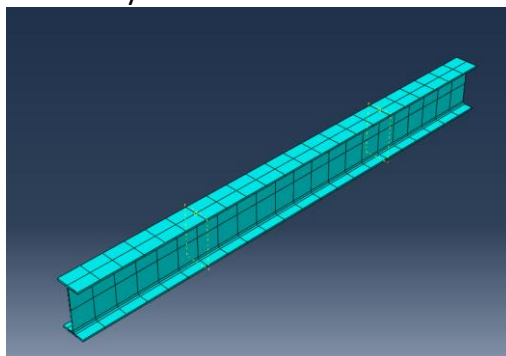


Figure 30. part of mesh

The last step is to create a job and submit it, but before that, so as to successfully extract the generated initial imperfection file, it is necessary to enter the text as shown in Figure 31 by editing keywords.

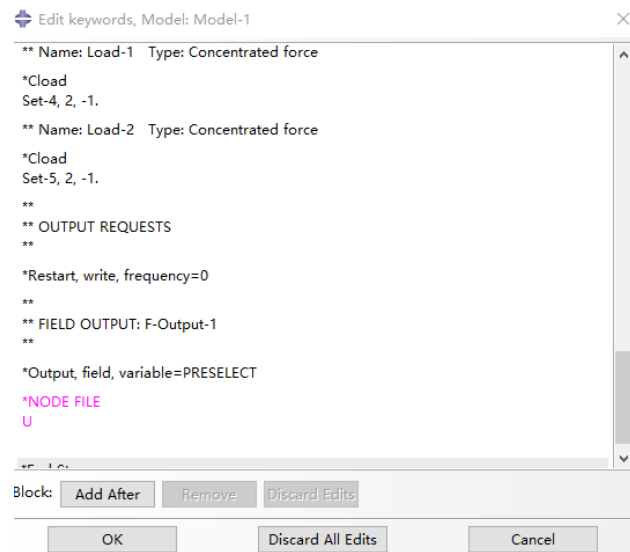


Figure 31. Initial imperfection file generation

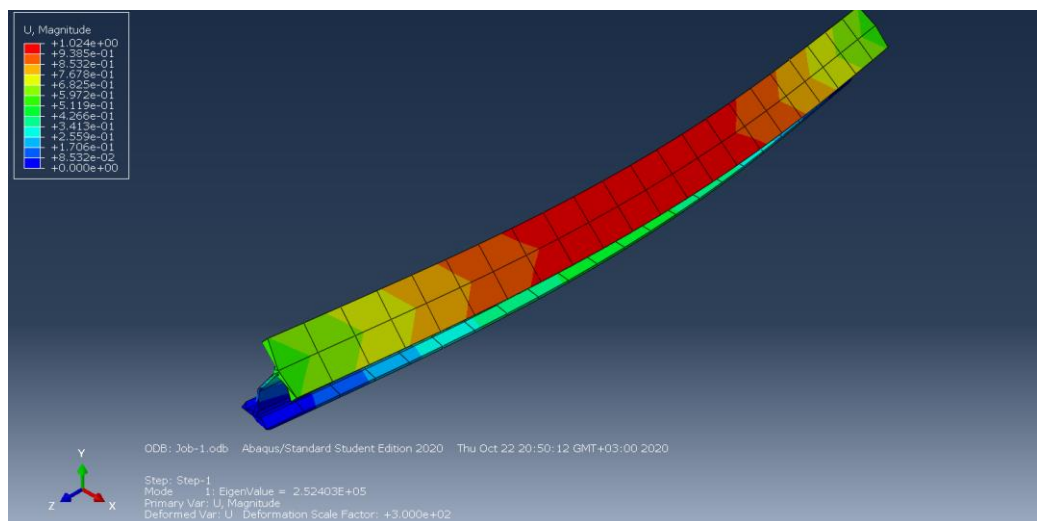


Figure 32. result of Eigenvalue buckling analysis

Completing the above steps represents the generation of the initial imperfection file. The next step is to adjust the copied model to carry out the import of the initial imperfection and the non-linear full-process analysis.

Change the material properties of the component in the copied model according to EN 1993 1-1: add yield strength and plastic strain in function-property, these values were from Table 3 and Table 4.

Data		
	Yield Stress	Plastic Strain
1	355	0
2	510	0.2

Figure 33. plastic property

Standard and steel grade	Nominal thickness of the element t [mm]			
	t ≤ 40 mm		40 mm < t ≤ 80 mm	
	f _y [N/mm ²]	f _u [N/mm ²]	f _y [N/mm ²]	f _u [N/mm ²]
EN 10025-2				
S 235	235	360	215	360
S 275	275	430	255	410
S 355	355	510	335	470
S 450	440	550	410	550

Table 3. Nominal values for Yield strength and Ultimate strength

Stress (MPa)	Strains	
	0	0
0	0	0
F _y = 355 MPa	$\varepsilon_1 = \frac{F_y}{E}$	0.00169
F _y = 355 MPa	$\varepsilon_2 = 0,025 - 5 \cdot \frac{F_u}{E}$	0.01286
F _u = 510 MPa	$\varepsilon_2 = 0,02 + 50 \cdot \frac{F_u - F_y}{E}$	0.05690
F _u = 510 MPa	∞	0.20

Table 4. Stress-strain relation

To obtain the limit value of the load proportionality factor, the descending section of the load-displacement curve needs to be obtained. Non-linear full process analysis adopts the arc length method of displacement control and correction: select General-Static, Riks in function-step.

Modify the inp file to add initial imperfection by using keywords edit as the Figure 34 shows:

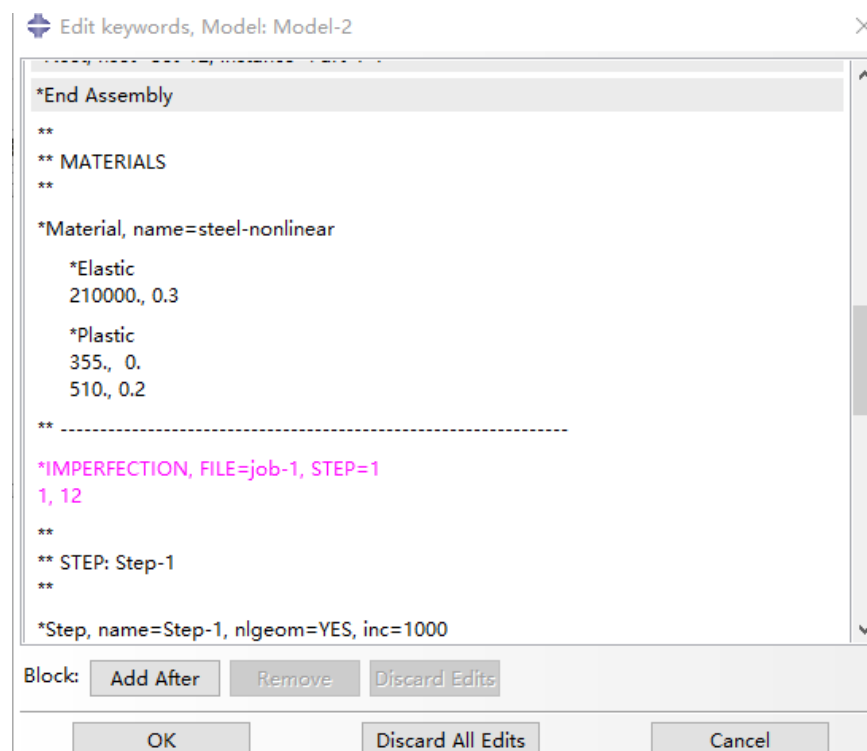


Figure 34. Import of initial imperfections

In Figure 34, 1 represents the first order buckling mode, and 12 is the imperfection factor, which needs to be adjusted accordingly. In this document, the initial imperfection was equal to the maximum node displacement of the first buckling mode multiplied by the imperfection factor. In this example, the maximum displacement is 1.024mm as shown in Figure 33. Therefore, in order to make the initial imperfection reach the pre-set value 12mm: according to the buckling curve a of IPE300 in EUROCODE, the value of imperfection in plastic analysis is $l/250$, so that the imperfection factor is 12.

Select the same boundary condition as before in function-load, but the eigenvalue obtained through Eigenvalue buckling analysis needs to be added in concentrated load, which is 252403N. Then just create and submit the job, and the whole analysis process is over.

5.3.4 Results and Discussions

This chapter main objective is to study the influence of increased imperfections on the stability of steel structure. A model with different imperfections were created and subjected to vertical loading on the selected nodes. Load-Displacement graphs were drawn after applying imperfections.

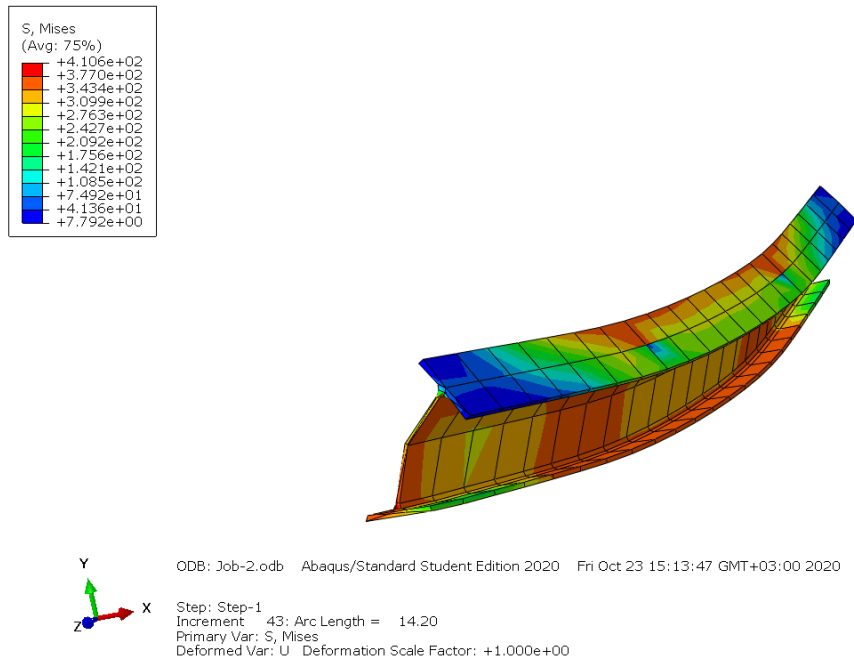


Figure 34. Deformed Shape of the model with 12mm imperfections

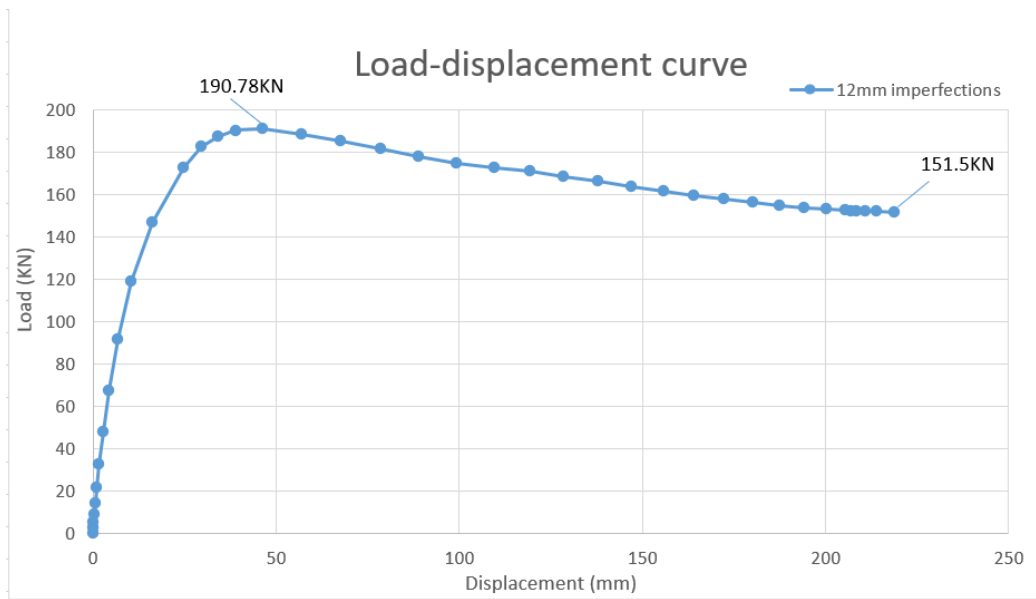


Figure 35. 12mm imperfections Load-displacement curve

Considering the maximum displacement in the middle part, the midpoint of Beam was selected as the node for observing the displacement in X direction. After the calculation was completed by the computer, the first 40 increments were used to make the curve.

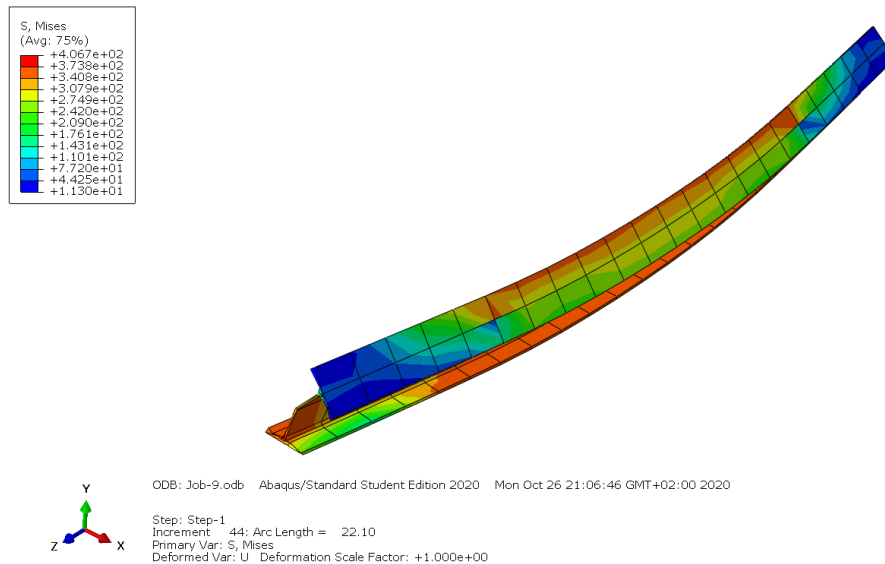


Figure 36. Deformed Shape of the model without imperfections

To better show the effect of imperfections on components, a model with obviously no initial imperfections was constructed to compare with models with imperfections.

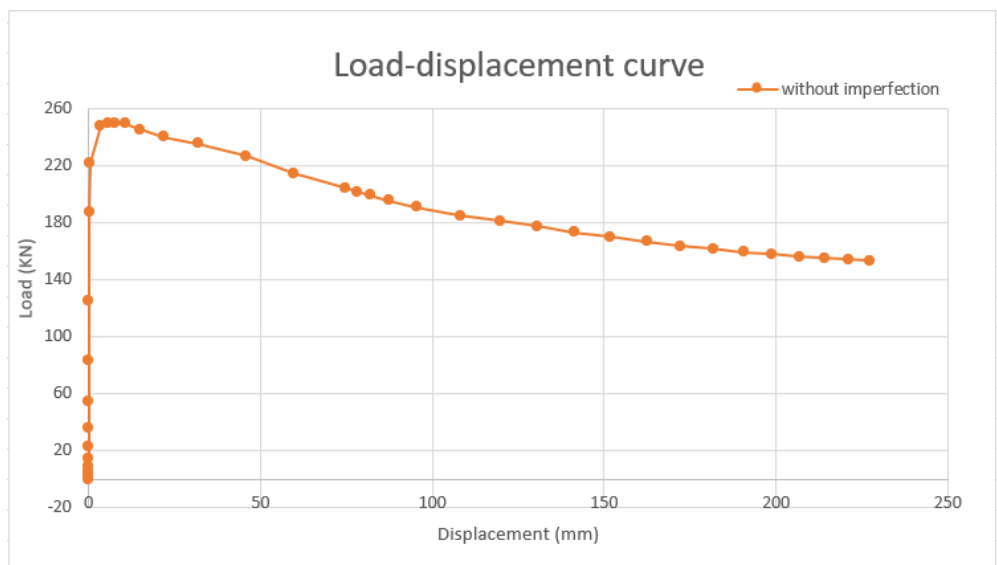


Figure 37. Load-displacement curve without imperfection

Figure 37 is the Load-displacement curve when there is no imperfection, which means that the Instability critical load value when there is no imperfection will be very close to the eigenvalue obtained in the previous Eigenvalue buckling analysis. Through the comparison between Figure 35 and Figure 37, it can be concluded that the existence of imperfections will reduce the stability of the component, thus, the value of critical load will become smaller.

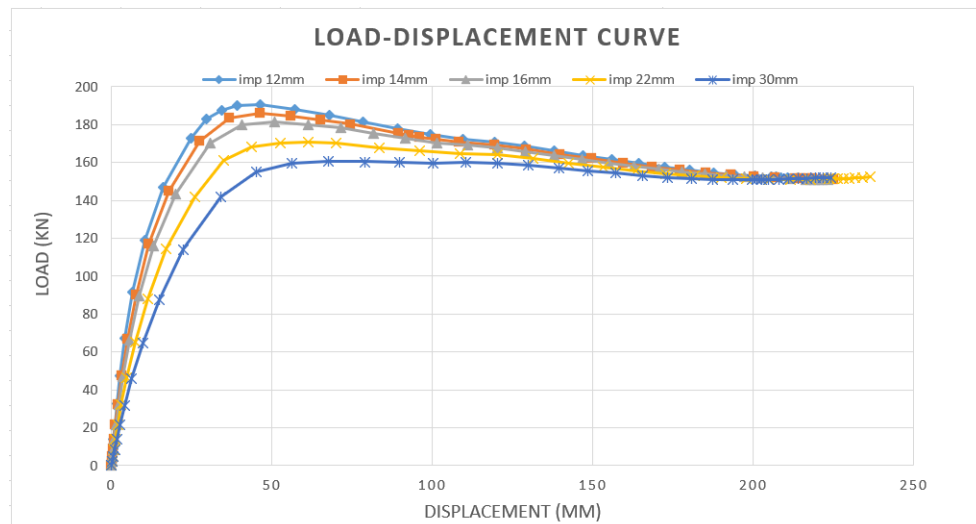


Figure 38. Load-displacement curve with different imperfections

To study how the increased imperfections will affect the stability of the steel component, a total of five models with different imperfections have been established in this simulation. Their imperfections were 12mm, 14mm, 16mm, 22mm and 30mm. All the data, deformed Shape diagrams of the remaining four models and their respective curves could be found in Appendix 1.

Through these analyses, it can be concluded that the stability of steel beams will gradually fail with the increased imperfections. The salient feature is that the stability and critical load decreases with the increase of imperfections, and the component is very sensitive to imperfections, even an increase of only 2mm of imperfections will cause the critical load of the component to decrease by about 5KN.

Since the model was constructed by the student version of ABAQUS, the mesh division was restricted by the upper limit of 1000 nodes, and could not be divided more accurately, which means that the accuracy of the analysis results of the model would be affected to a certain extent. And due to the limitations of the equipment, the reliability of the model could not be verified through experiments. Therefore, the accuracy of the data was determined by manual calculation according to the Eurocode, When the imperfection is 12mm, the manually calculated critical load value is 200.04KN, which is slightly larger than the value calculated by the software, but the error within 5%, the data accuracy of the model has been considered credible. The specific calculation could be found in Appendix 2.

6 CONCLUSION

The aim of this thesis was to collect methods for detecting residual stresses and geometric imperfections through literature review, and to describe the analysis process of reused steel structure stability through nonlinear buckling analysis of compressed steel beams.

Considering the results obtained in this thesis and linking with the application prospects of reused steel structures, it can also be concluded that:

Since the stability of compression steel components will rapidly weaken due to the increased imperfection, when using reused steel components as compression components, it is necessary to detect the geometric imperfections and their residual stress.

Because the reusable steel structure will have increased defects due to thermal cutting, re-welding, transportation, deconstruction and reconstruction. The performance of the reusable steel structure should be re-evaluated and designed based on the increase imperfections.

Buckling analysis in engineering is mainly to study the stability of a structure under a specific load and to determine the critical load for structural instability. Especially for nonlinear buckling analysis, the results produced by nonlinear buckling analysis are more accurate than linear analysis. The analysis can be carried out easily through finite element analysis software such as ABAQUS. For the reused steel structures, how to ensure their stability is a very important matter, and finite element analysis software will be a very useful analysis tool for this.

Finally, It is hoped that this thesis will provide a reference for those who wish to obtain information on how to use finite element analysis software to analyse and process the measurement data of geometric imperfections and residual stress of the reused steel structures.

REFERENCES

- (1) FU Xue-yi, LIU Li(Technical Canter of Baotou Steel, 2006). Harmfulness of Residual Stress and Countermeasures.
- (2) Flaman, M.T. and Herring, J.A., "Comparison of Four Hole-Producing Techniques for the Centre-Hole Residual Stress Measurement Method," Experimental Techniques, Vol. 9, No. 8, 1985
- (3) Flaman, M.T., Herring, J.A., "Ultra-High-Speed Centre-Hole Technique for Difficult Machining Materials," Experimental Techniques, Vol. 10, No. 1, Jan 1986, pp 34-35
- (4) A. Ajovalasit, Michele Scafidi, Bernardo Zuccarello, M. Beghini. 2010 The hole-drilling strain gauge method for the measurement of uniform or non-uniform residual stresses Working Group on Residual Stresses
- (5) Lars Fuglsang Andersen. 2000 Residual stresses and deformations in steel structures
- (6) Bijak-Zochowski, M.A Semi Destructive Method of Measuring Residual Stresses.1978
- (7) Schajer, G.S., "Application of Finite Element Calculations to Residual Stress Measurements," 1981
- (8) Schajer, G.S., "Measurement of Non-Uniform Residual Stresses Using the Hole-Drilling Method. 1988
- (9) N. Tebedge, GA Alpsten and L. Tall Residual stress measurement by the sectioning method, presented at SESA Spring Meeting, 1972
- (10) N. Ralakovsky, THE STUDY OF INTERNAL STRESSES IN CAST IRON AND STEEL, London, 1888
- (11) Manual on Stability of Steel Structures, ECCS Committee 8 - Stability 1976
- (12) Xi Zhao 2016, MEASUREMENT AND APPLICATION OF GEOMETRIC IMPERFECTIONS IN COLD-FORMED STEEL MEMBERS

- (13) M. Tootkaboni, B.W. Schafer and X.Zhao, 2015, Development of a Laser-Based Geometric Imperfection Measurement Platform with Application to Cold-Formed Steel Construction
- (14) Amar Khennane 2013, Introduction to Finite Element Analysis Using MATLAB® and Abaqus
- (15) Li Wei-long 2013, Test of residual stress by hole drilling strain method
- (16) G.Anwar 2015 Assessment and validation of an Ayrton-Perry design methodology for the verification of flexural and lateral-torsional buckling of prismatic

APPENDIX 1 RESULTS OF BUCKLING ANALYSIS IN ABAQUS

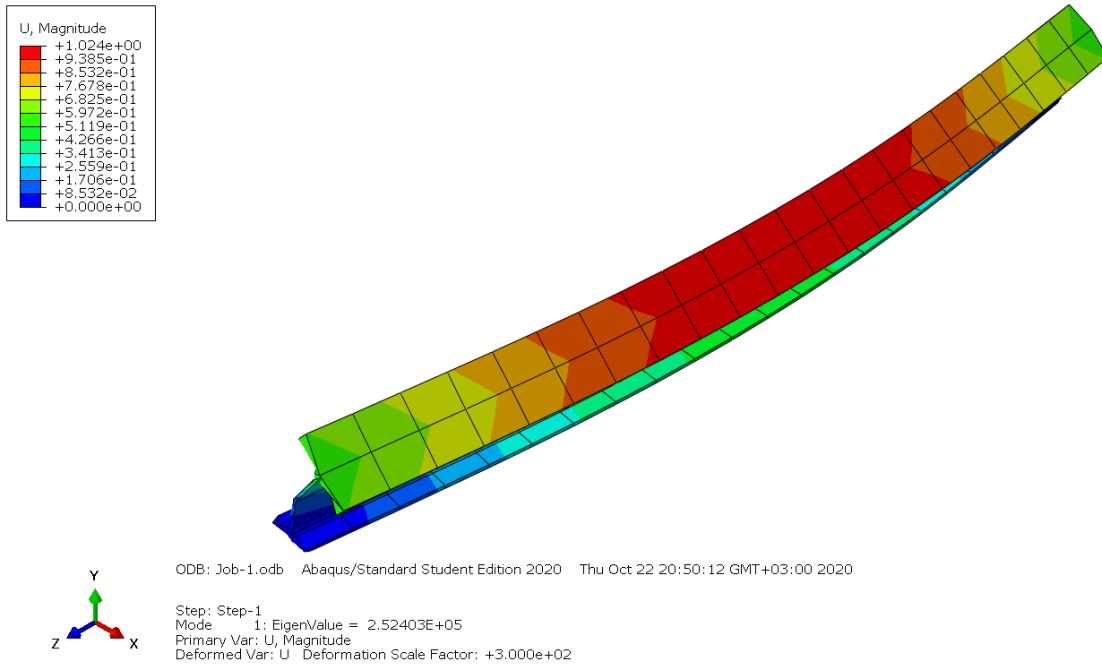


Figure 1.1 Buckling mode 1 and buckling critical load 252.403KN

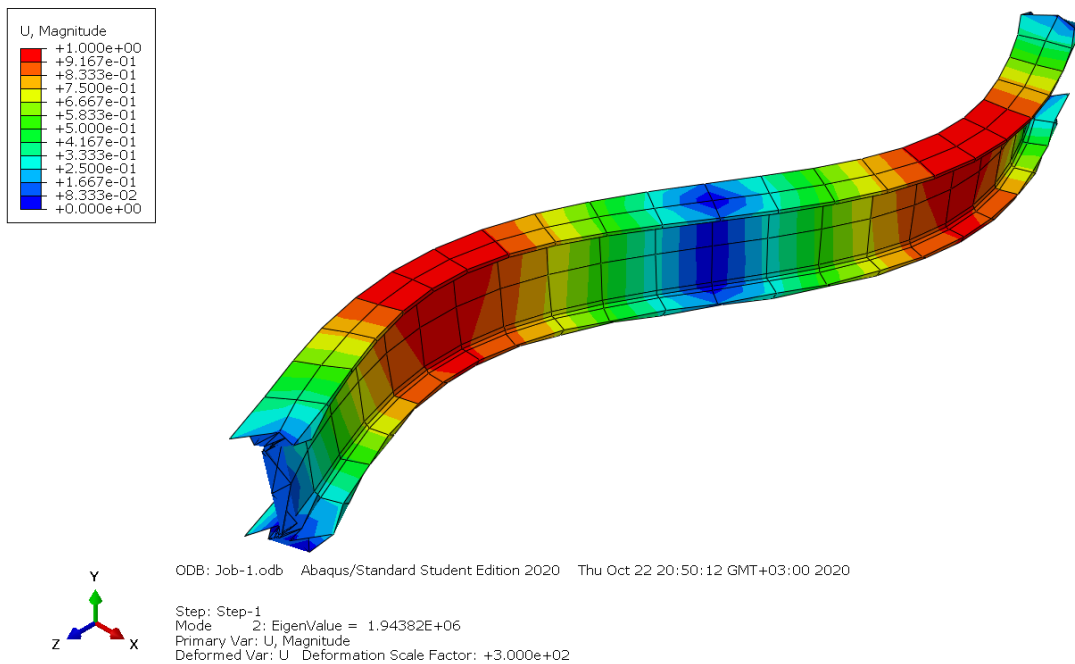


Figure 1.2 Buckling mode 2

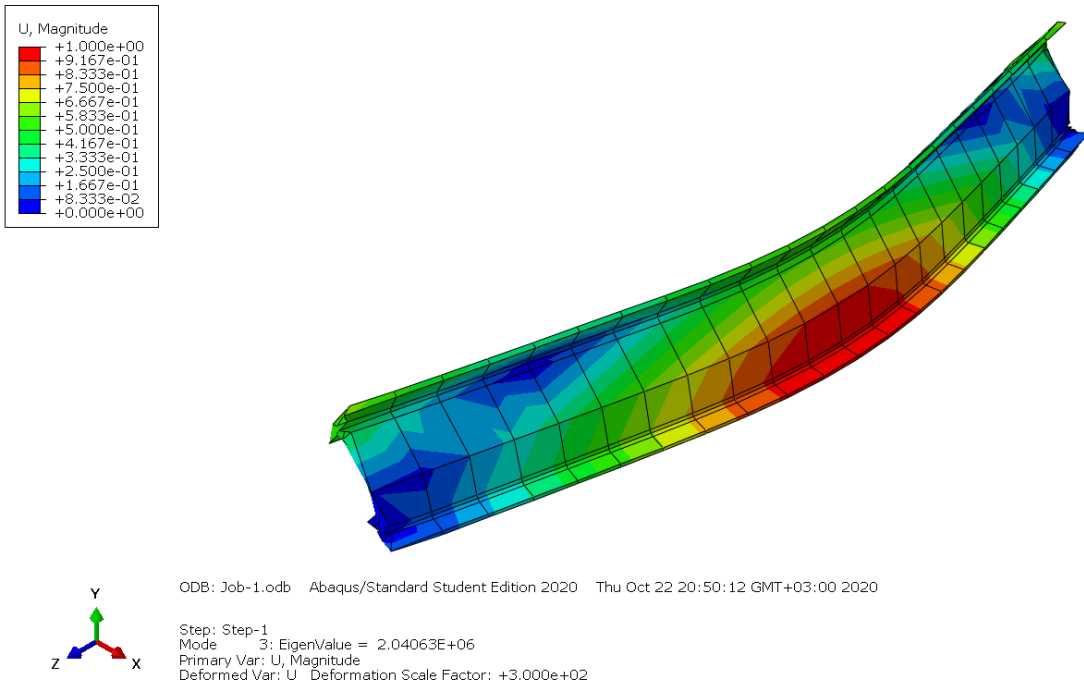


Figure 1.3 Buckling mode 3

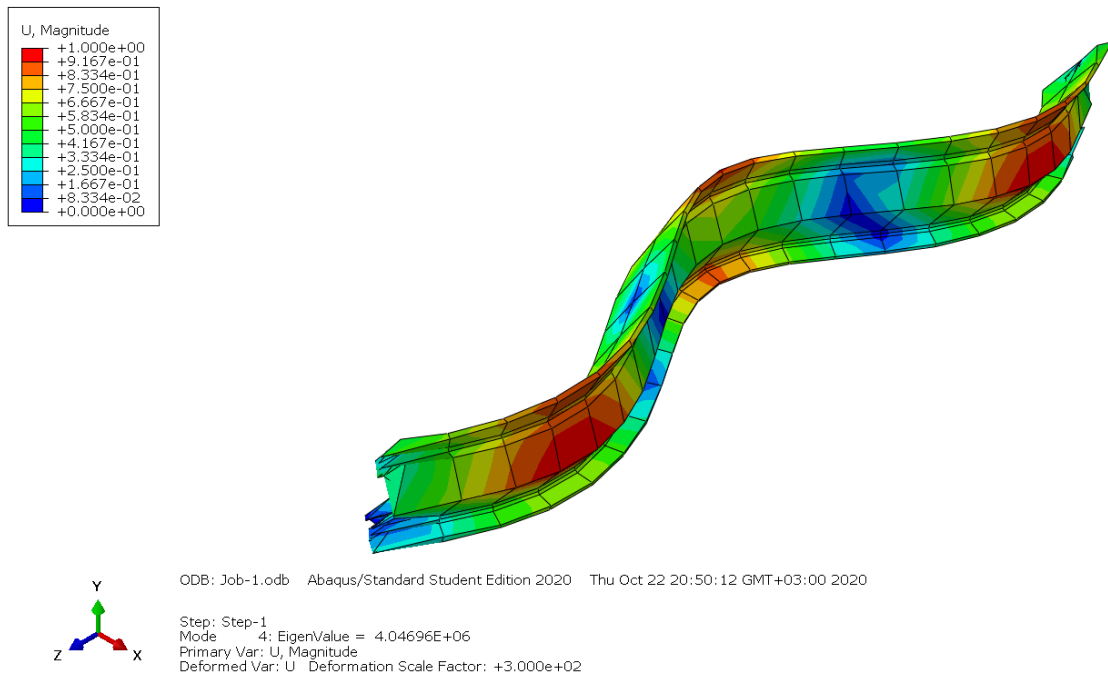


Figure 1.4 Buckling mode 4

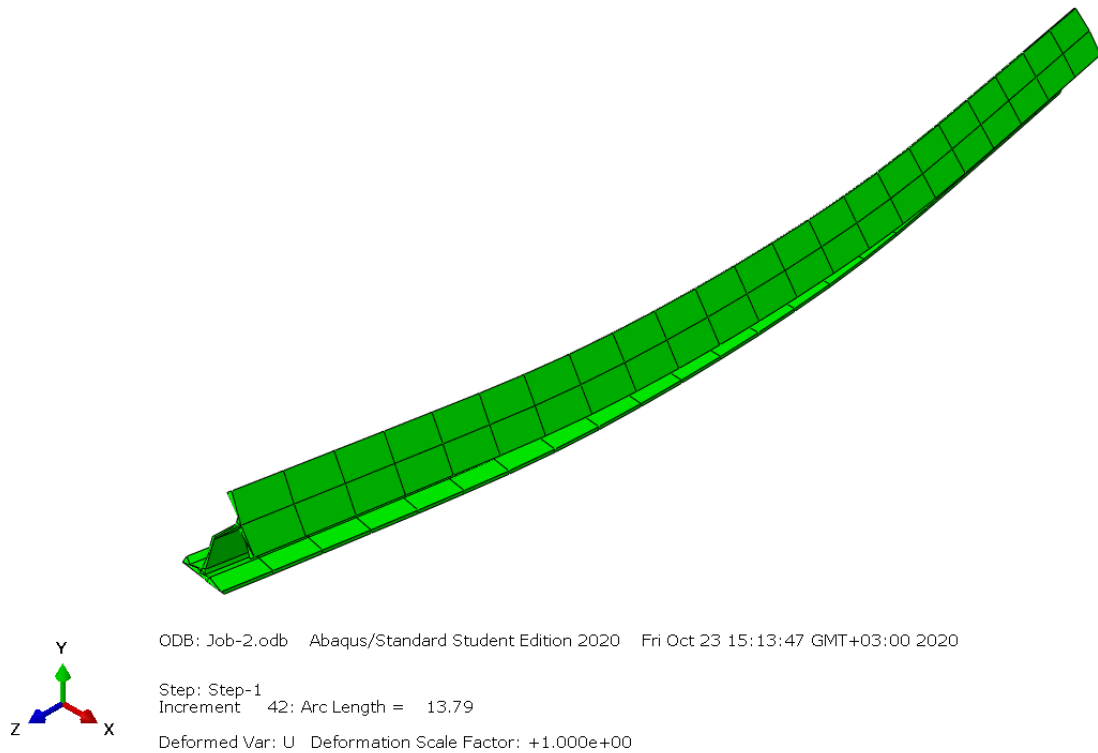


Figure 1.5 Deformed Shape of the model with 12mm imperfections

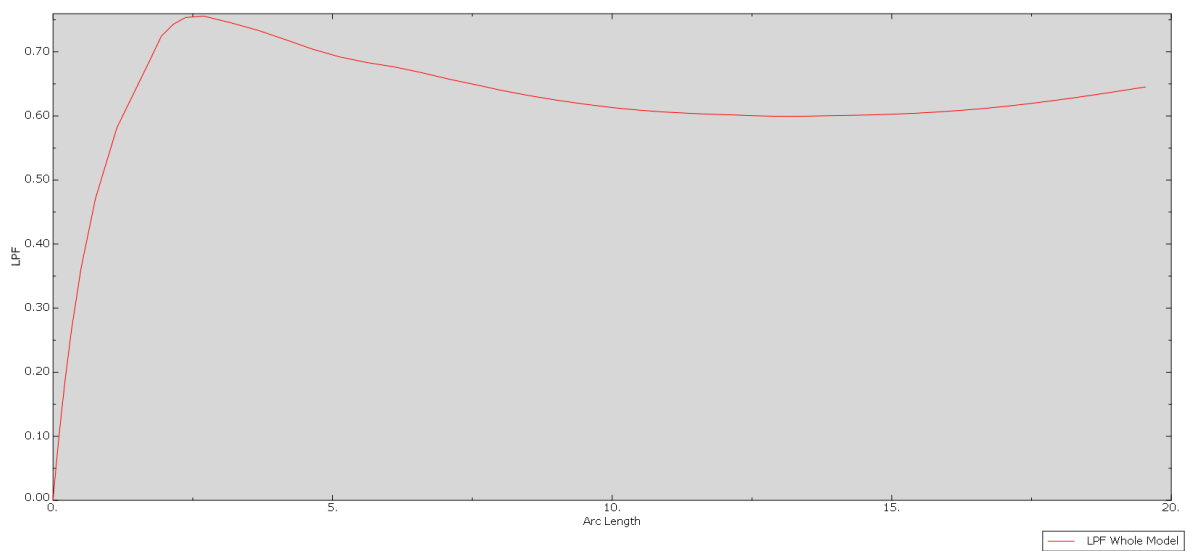


Figure 1.6 Load proportionality Factor in the model with 12mm imperfections

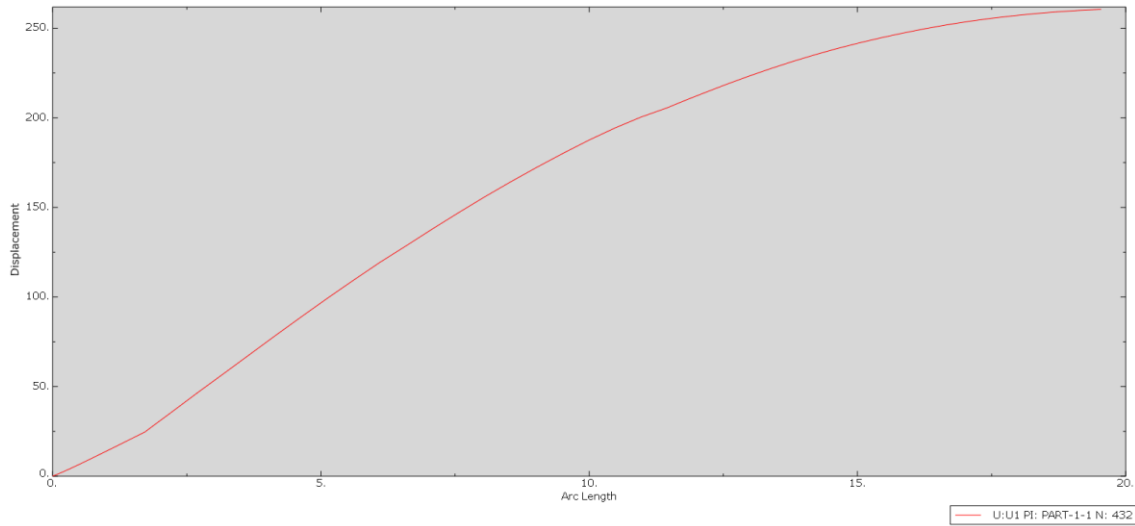


Figure 1.7 Displacement(mm) in the midpoint of model with 12mm imperfections

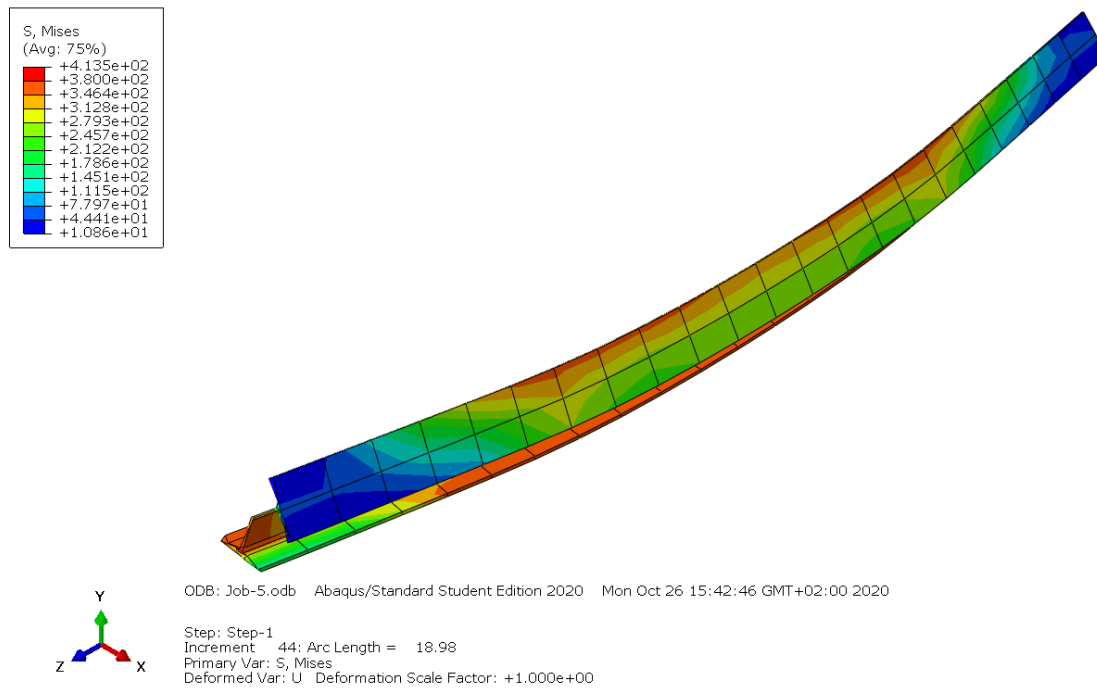


Figure 1.8 Deformed Shape of the model with 14mm imperfections

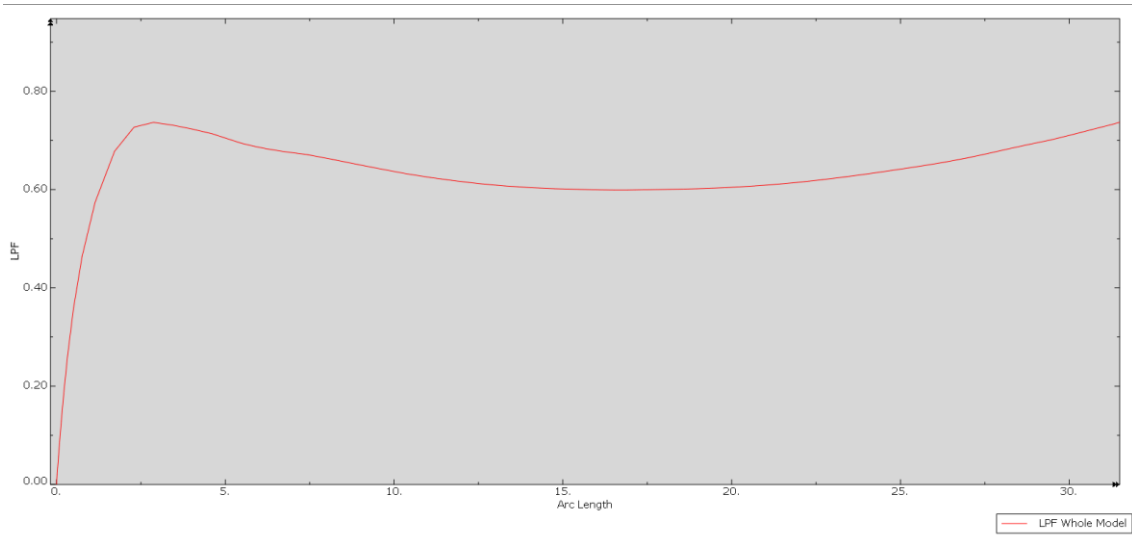


Figure 1.6 Load proportionality Factor in the model with 14mm imperfections

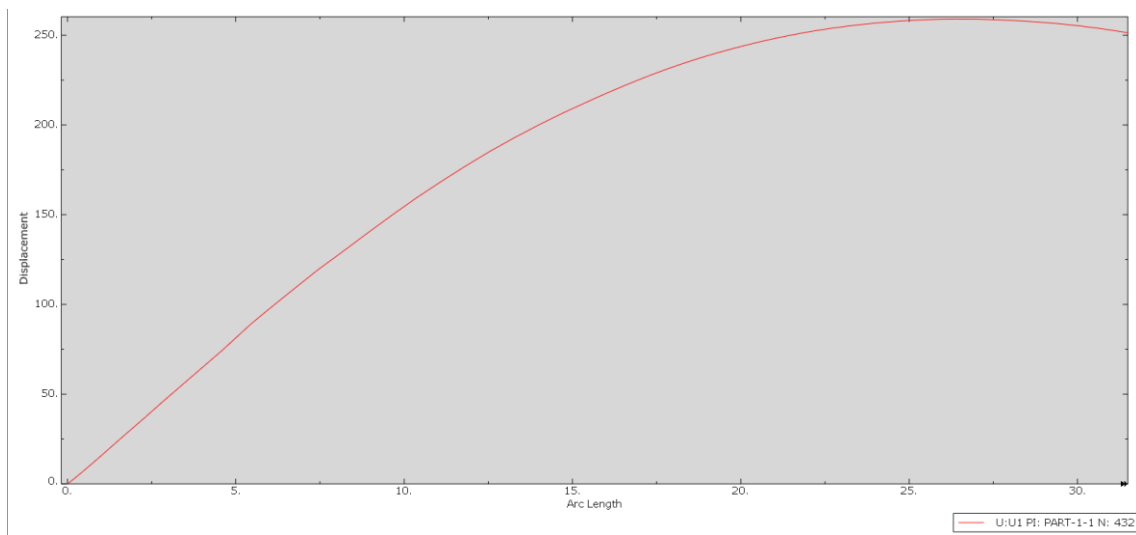


Figure 1.10 Displacement(mm) in the midpoint of model with 14mm imperfections

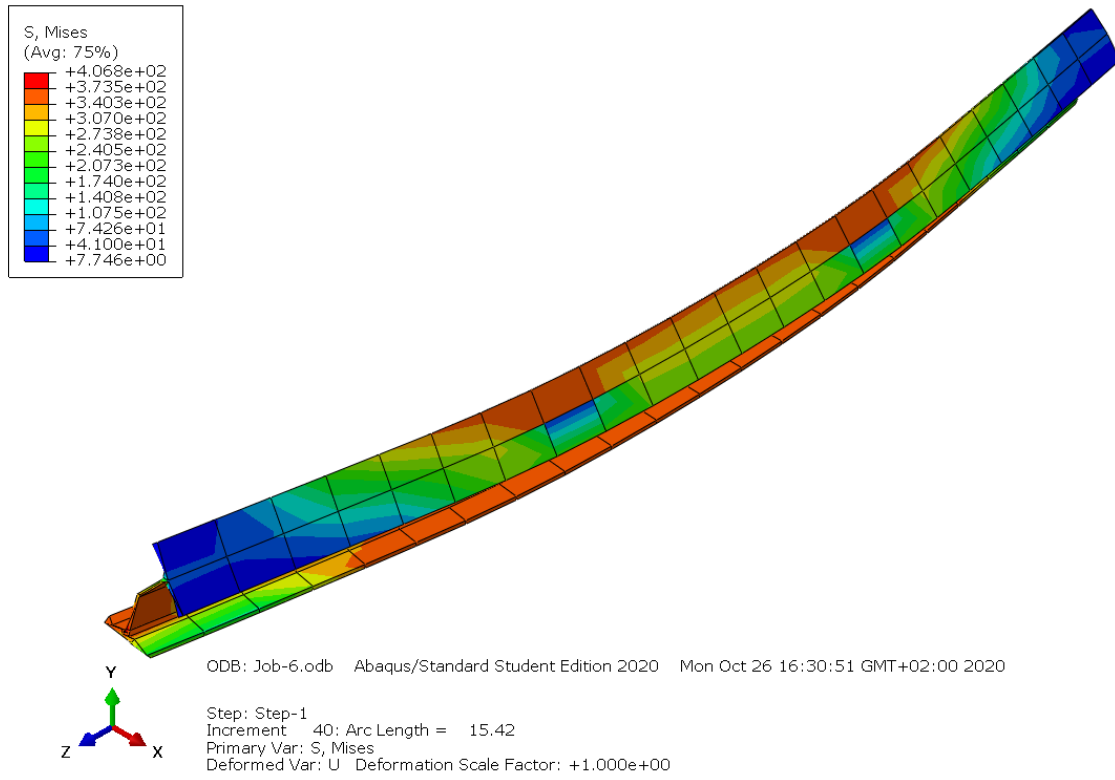


Figure 1.11 Deformed Shape of the model with 16mm imperfections

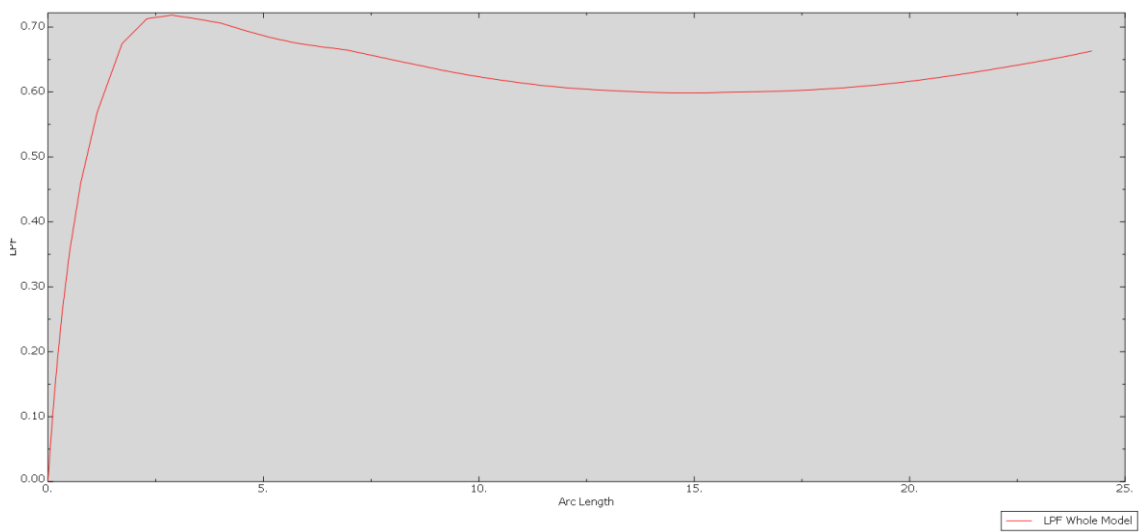


Figure 1.12 Load proportionality Factor in the model with 16mm imperfections

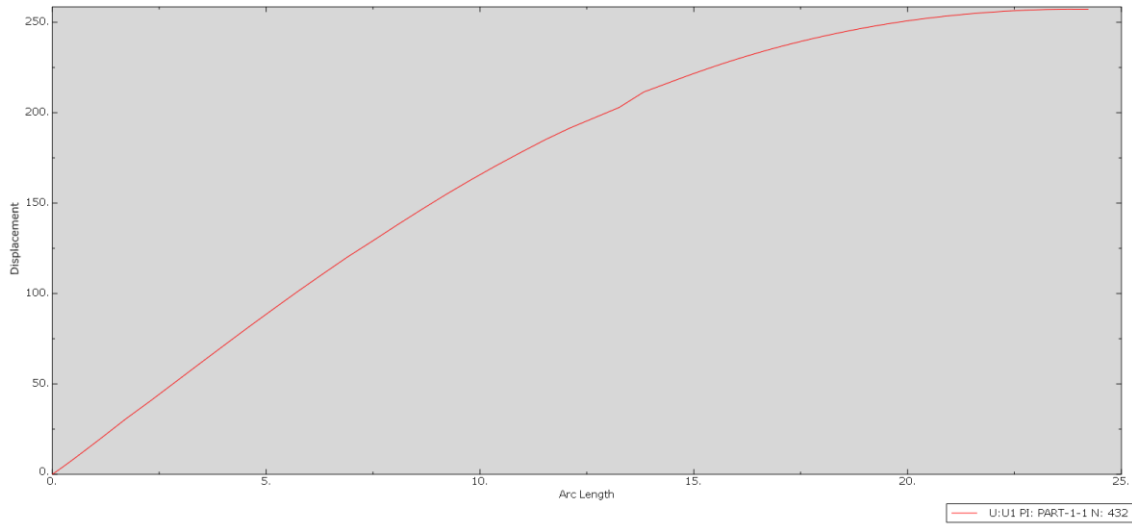


Figure 1.13 Displacement(mm) in the midpoint of model with 16mm imperfections

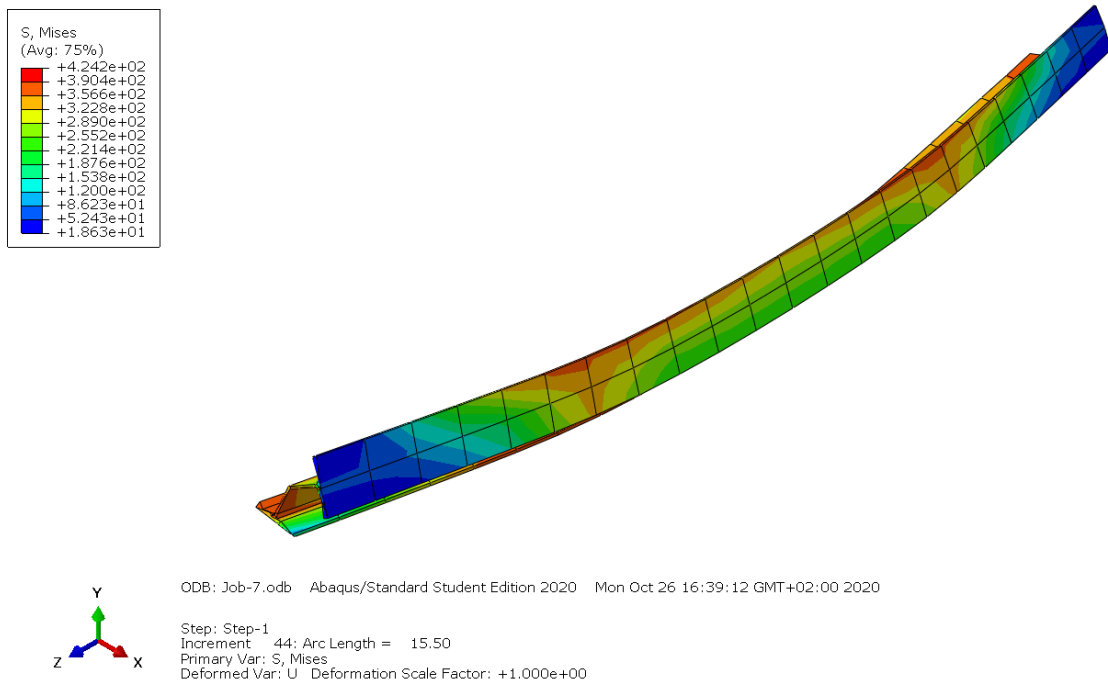


Figure 1.14 Deformed Shape of the model with 22mm imperfections

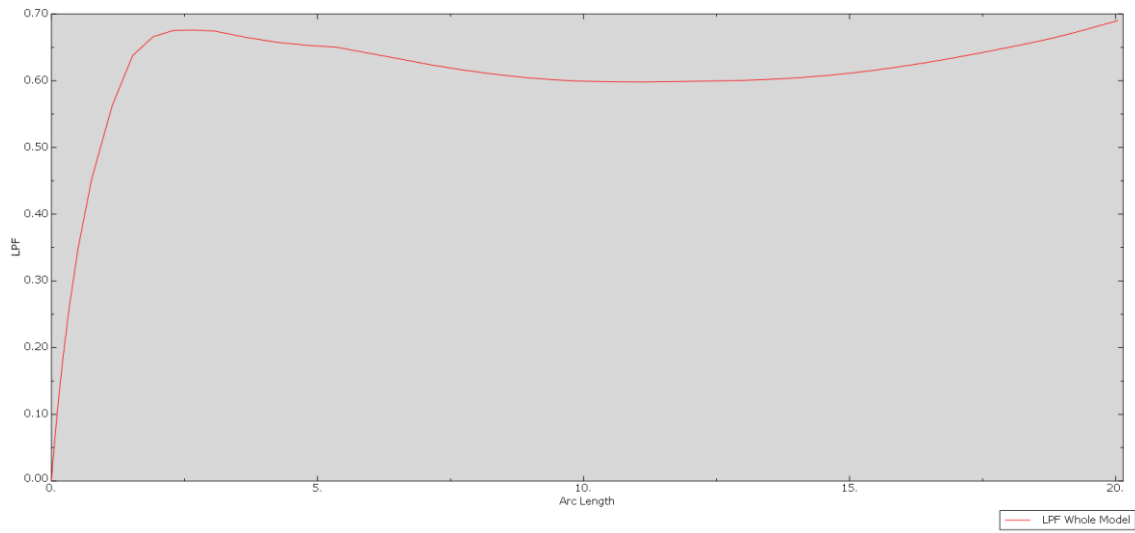


Figure 1.15 Load proportionality Factor in the model with 22mm imperfections

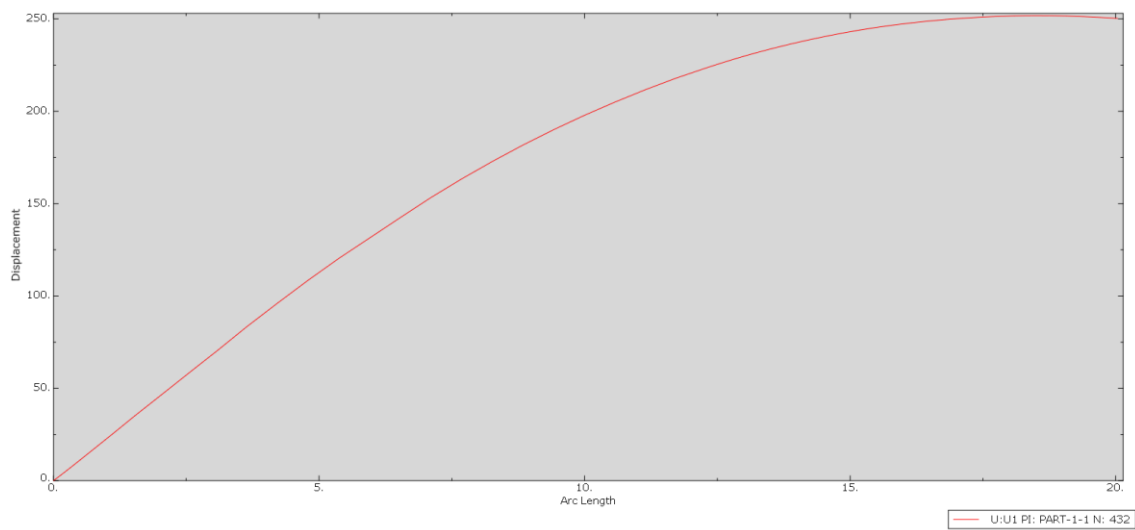


Figure 1.16 Displacement(mm) in the midpoint of model with 22mm imperfections

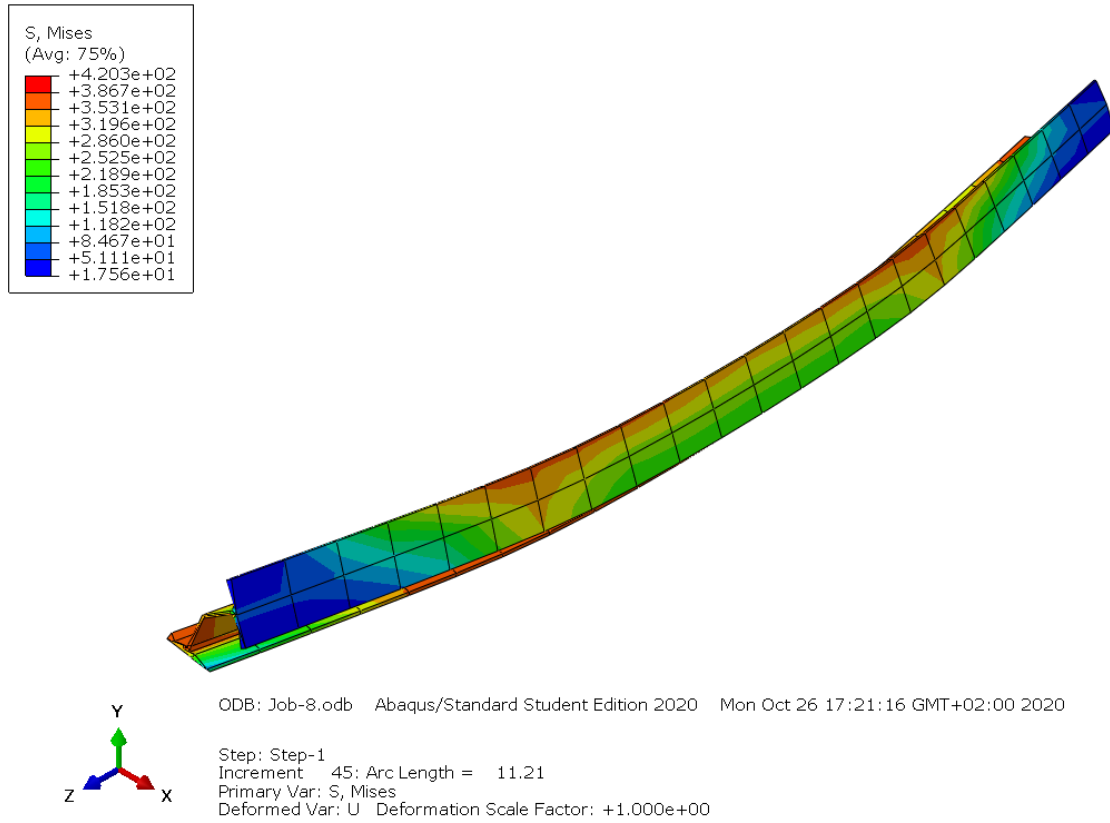


Figure 1.17 Deformed Shape of the model with 30mm imperfections

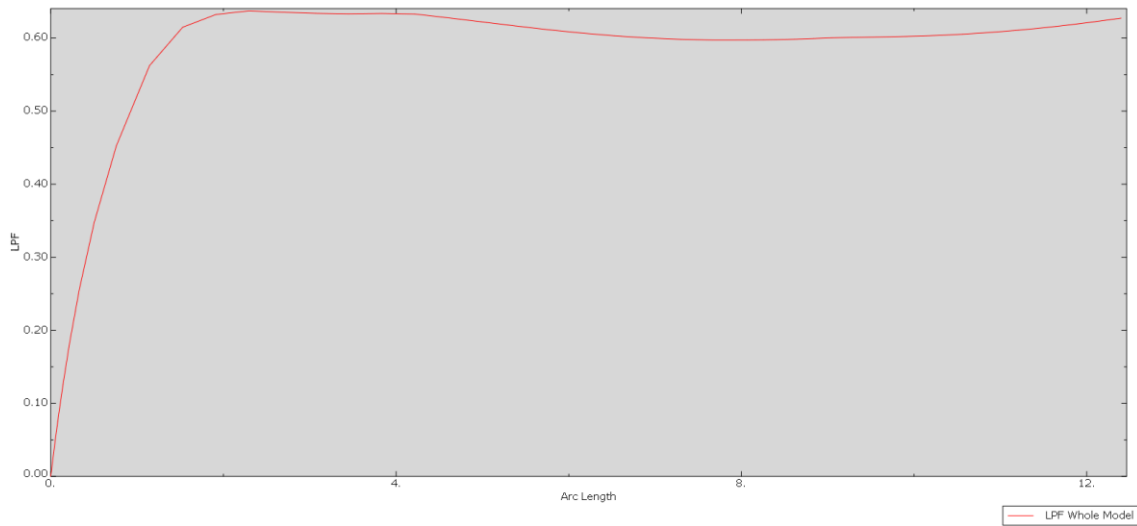


Figure 1.18 Load proportionality Factor in the model with 30mm imperfections

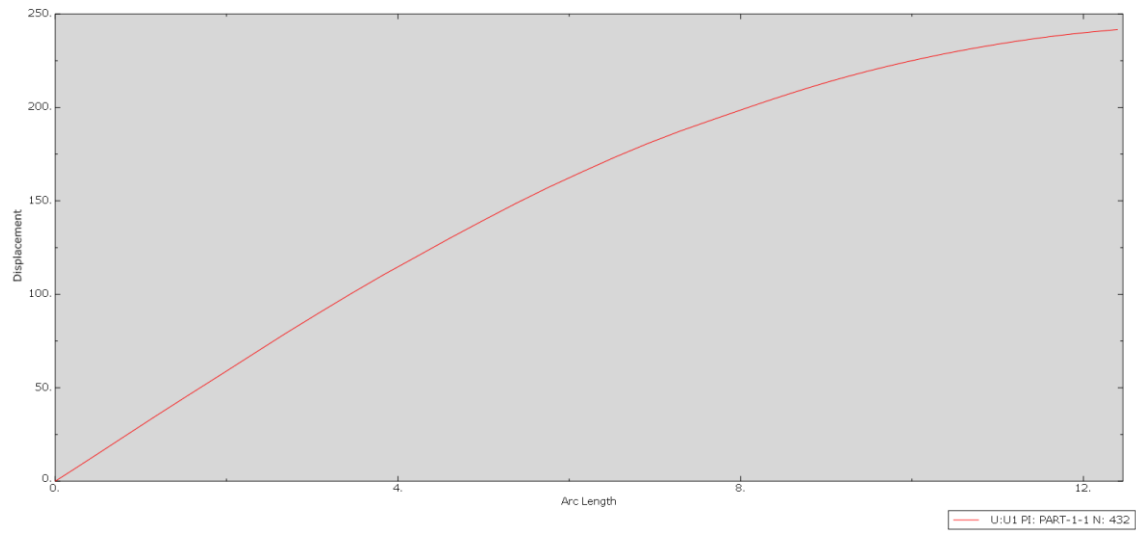


Figure 1.19 Displacement(mm) in the midpoint of model with 30mm imperfections

Number	increment point data of displacement and Load					
	12mm Imperfections			14mm Imperfections		
	DISPLACEMENT(mm)	LPF	LOAD(KN)	DISPLACEMENT(mm)	LPF	LOAD(KN)
1	0	0	0	0	0	0
2	0.118596	0.009937	2.508106	0.13794	0.009931	2.506584
3	0.238023	0.019747	4.984303	0.276668	0.019724	4.978346
4	0.418687	0.034228	8.639174	0.486198	0.034157	8.621405
5	0.693001	0.055422	13.98868	0.803601	0.05524	13.94284
6	1.11156	0.086047	21.71842	1.28628	0.08562	21.61082
7	1.75405	0.12943	32.66852	2.0237	0.128505	32.43505
8	2.74724	0.188959	47.69382	3.15635	0.187108	47.22662
9	4.28982	0.267045	67.40296	4.90193	0.263716	66.56271
10	6.68897	0.362906	91.59856	7.59428	0.357666	90.27597
11	10.4006	0.470971	118.8745	11.7295	0.46399	117.1125
12	16.0828	0.581783	146.8438	18.0303	0.573977	144.8735
13	24.6778	0.684728	172.8274	27.5521	0.67784	171.0888
14	29.5277	0.724342	182.8261	36.9	0.726928	183.4788
15	34.3061	0.743142	187.5713	46.4935	0.736671	185.938
16	39.149	0.753593	190.2091	55.8419	0.730934	184.4899
17	46.4269	0.755857	190.7806	65.1868	0.722958	182.4768
18	57.0745	0.745408	188.1432	74.5237	0.7137	180.14
19	67.7839	0.733631	185.1707	89.3951	0.694428	175.2757
20	78.5104	0.719211	181.531	92.7485	0.690775	174.3537
21	89.0338	0.704271	177.7601	96.0809	0.687403	173.5026
22	99.4049	0.692144	174.6992	101.04	0.682926	172.3726
23	109.473	0.683356	172.4811	108.395	0.677488	171
24	119.326	0.676578	170.7703	119.327	0.670922	169.3427
25	128.508	0.667678	168.5239	129.361	0.66144	166.9494
26	137.859	0.657641	165.9906	139.614	0.651329	164.3974
27	146.93	0.648702	163.7343	149.642	0.64157	161.9342
28	155.759	0.639435	161.3953	159.334	0.632185	159.5654
29	164.182	0.631459	159.3821	168.392	0.624334	157.5838
30	172.287	0.624483	157.6214	177.09	0.617646	155.8957
31	180.053	0.618423	156.0918	185.328	0.611817	154.4244
32	187.479	0.613115	154.7521	192.975	0.607351	153.2972
33	194.288	0.609018	153.718	200.163	0.604031	152.4592
34	200.389	0.605958	152.9456	206.888	0.601729	151.8782
35	205.549	0.603839	152.4108	213.156	0.600389	151.54
36	207.066	0.603342	152.2853	214.714	0.600105	151.4683
37	208.561	0.602907	152.1755	216.246	0.599777	151.3855
38	210.762	0.602306	152.0238	218.497	0.599358	151.2798
39	213.973	0.601614	151.8492	221.769	0.598971	151.1821
40	218.714	0.600224	151.4983	224.915	0.598997	151.1886

Table 1.1 increment point data of displacement and Load in 12mm and 14mm Imperfections

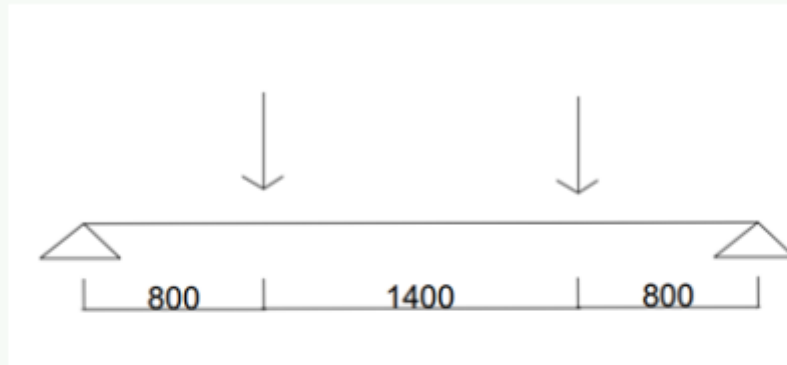
Number	increment point data of displacement and Load					
	16mm Imperfections			22mm Imperfections		
	DISPLACEMENT(mm)	LPF	LOAD(KN)	DISPLACEMENT(mm)	LPF	LOAD(KN)
1	0	0	0	0	0	0
2	0.157163	0.009926	2.505435	0.213994	0.009918	2.503436
3	0.315069	0.019706	4.973854	0.428605	0.019675	4.96608
4	0.553276	0.034105	8.608129	0.751632	0.034014	8.585286
5	0.913488	0.055106	13.90887	1.23854	0.054876	13.85092
6	1.45989	0.085307	21.53177	1.97381	0.084781	21.39888
7	2.29179	0.127834	32.26569	3.08659	0.126698	31.97896
8	3.56371	0.185787	46.8932	4.77418	0.183666	46.35785
9	5.5133	0.261386	65.97461	7.33746	0.25777	65.06192
10	8.50308	0.354077	89.3701	11.2307	0.34877	88.03059
11	13.0723	0.459328	115.9358	17.1304	0.452979	114.3333
12	20.0109	0.568855	143.5807	26.0062	0.562532	141.9848
13	30.6473	0.674427	170.2274	35.0222	0.637668	160.9493
14	40.6171	0.712871	179.9308	43.7509	0.665864	168.0661
15	50.9223	0.718299	181.3008	52.5147	0.675449	170.4854
16	61.238	0.712625	179.8687	61.2836	0.676027	170.6312
17	71.4577	0.705773	178.1392	69.9647	0.67448	170.2408
18	81.639	0.693987	175.1644	83.4088	0.665235	167.9073
19	91.5679	0.683609	172.545	96.1283	0.657816	166.0347
20	101.385	0.675325	170.4541	108.529	0.653178	164.8641
21	110.902	0.669675	169.028	120.332	0.650085	164.0834
22	120.263	0.664975	167.8417	131.33	0.64144	161.9014
23	128.959	0.656846	165.7899	142.345	0.633035	159.7799
24	137.848	0.648518	163.6879	153.202	0.624221	157.5553
25	146.491	0.640635	161.6982	163.262	0.616745	155.6683
26	154.876	0.632622	159.6757	172.71	0.610453	154.0802
27	162.88	0.625661	157.9187	181.605	0.605307	152.7813
28	170.54	0.619618	156.3934	189.91	0.60155	151.833
29	177.862	0.61426	155.0411	197.658	0.599249	151.2522
30	184.967	0.609594	153.8634	204.854	0.598235	150.9963
31	191.434	0.60603	152.9638	211.619	0.598012	150.94
32	197.12	0.603457	152.3144	217.861	0.598576	151.0824
33	202.814	0.601522	151.826	223.486	0.599483	151.3113
34	211.377	0.599648	151.353	224.837	0.599708	151.3681
35	216.448	0.598876	151.1581	226.159	0.599859	151.4062
36	217.729	0.598762	151.1293	228.083	0.600205	151.4935
37	218.99	0.59868	151.1086	229.91	0.600622	151.5988
38	220.232	0.598647	151.1003	231.651	0.601192	151.7427
39	221.455	0.598666	151.1051	234.116	0.602227	152.0039
40	223.257	0.598748	151.1258	236.413	0.603634	152.359

Table 1.2 increment point data of displacement and Load in 16mm and 22mm Imperfections

Number	increment point data of displacement and Load					
	without Imperfections			30mm Imperfections		
	DISPLACEMENT(mm)	LPF	LOAD(KN)	DISPLACEMENT(mm)	LPF	LOAD(KN)
1	0	0	0	0	0	0
2	0.00031083	0.009997	2.523321	0.287374	0.009915	2.502477
3	0.00063204	0.019989	5.045233	0.575238	0.019661	4.962369
4	0.00113404	0.034966	8.825422	1.00791	0.033972	8.574609
5	0.00193492	0.057407	14.48975	1.65877	0.054771	13.82444
6	0.00325297	0.091016	22.97281	2.63886	0.084548	21.34017
7	0.00552728	0.141311	35.66732	4.11661	0.126232	31.86134
8	0.00975035	0.216483	54.64096	6.34712	0.182846	46.15088
9	0.0185799	0.328638	82.94922	9.71632	0.256563	64.75727
10	0.0413943	0.495511	125.0685	14.8035	0.347492	87.70802
11	0.143126	0.742635	187.4433	22.4691	0.452341	114.1722
12	0.390603	0.878215	221.6641	33.9541	0.562214	141.9045
13	3.6007	0.981728	247.7911	45.2252	0.614816	155.1814
14	5.58843	0.987489	249.2452	56.3643	0.632205	159.5704
15	7.57643	0.989999	249.8787	67.6097	0.637265	160.8476
16	10.5617	0.987766	249.3151	78.8325	0.635324	160.3577
17	15.0435	0.971208	245.1358	89.6502	0.633855	159.9869
18	21.765	0.951288	240.1079	100.247	0.633162	159.812
19	31.8005	0.932995	235.4907	110.496	0.633705	159.949
20	45.9032	0.898628	226.8164	120.187	0.632868	159.7378
21	59.6697	0.849409	214.3934	129.943	0.627673	158.4265
22	74.644	0.808418	204.0471	139.33	0.622237	157.0545
23	78.2862	0.79897	201.6624	148.524	0.61675	155.6696
24	81.9364	0.788773	199.0887	157.217	0.611496	154.3434
25	87.3935	0.774687	195.5333	165.326	0.60695	153.196
26	95.495	0.756263	190.883	173.226	0.603087	152.221
27	108.136	0.733058	185.026	180.584	0.600203	151.493
28	119.896	0.716159	180.7607	187.342	0.598234	150.9961
29	130.73	0.701793	177.1347	193.518	0.597229	150.7424
30	141.29	0.686366	173.2408	199.589	0.597282	150.7558
31	151.983	0.673005	169.8685	201.088	0.597392	150.7835
32	162.455	0.659592	166.483	202.583	0.597502	150.8113
33	172.336	0.648458	163.6727	204.78	0.597771	150.8792
34	181.804	0.63889	161.2578	207.978	0.598382	151.0334
35	190.652	0.6309	159.2411	211.061	0.599285	151.2613
36	198.984	0.624132	157.5328	213.997	0.600282	151.513
37	206.813	0.618269	156.053	216.75	0.600829	151.651
38	214.171	0.61359	154.872	219.363	0.60122	151.7497
39	221.028	0.610088	153.988	221.82	0.601652	151.8588
40	227.473	0.606678	153.1273	224.137	0.602242	152.0077

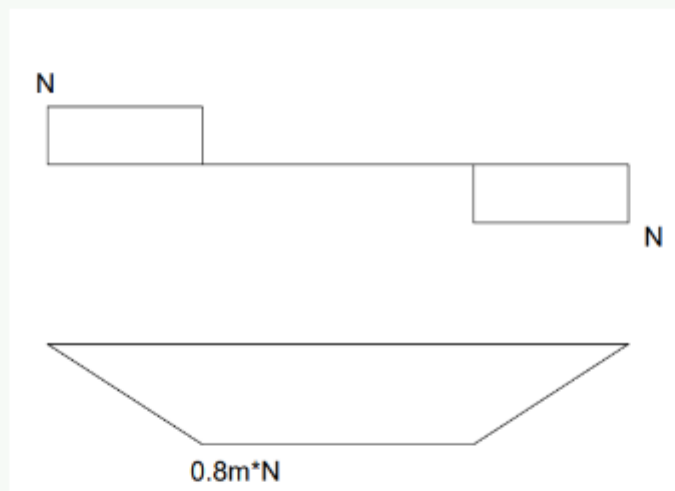
Table 1.3 increment point data of displacement and Load in Omm and 30mm Imperfections

APPENDIX 2 LATERAL TORSIONAL BUCKLING RESISTANCE CALCULATION



PROFILE: IPE300

shear and moment diagram



material and crosssection property:

$$E := 210000 \text{ MPa}$$

$$C_1 := 1.04$$

$$G := 81000 \text{ MPa}$$

$$k_w := 1 \quad k := 1$$

$$I_t := 20.2 \text{ cm}^4$$

$$I_w := 125900 \text{ cm}^6$$

$$L := 3000 \text{ mm}$$

$$\gamma_{m1} := 1$$

$$I_z := 604 \text{ cm}^4$$

$$W_y := 628 \text{ cm}^3 \quad f_y := 355 \text{ MPa}$$

$$L_{cr} := k \cdot L = 3 \text{ m}$$

Lateral torsional buckling resistance calculation

$$M_{CR} := C_1 \cdot \frac{3.14^2 \cdot E \cdot I_z}{L_{cr}^2} \cdot \left(\sqrt{\left(\frac{k}{k_w} \right)^2 \cdot \frac{I_w}{I_z} + \frac{L_{cr}^2 \cdot G \cdot I_t}{3.14^2 \cdot E \cdot I_z}} \right) = 261.002 \text{ m} \cdot \text{kN}$$

$$\lambda_{LT} := \sqrt{\frac{W_y \cdot f_y}{M_{CR}}} = 0.924$$

Imperfection factor α_{LT}

Table 6.4: Recommended values for lateral torsional buckling curves for cross-sections using equation (6.56)

Cross-section	Limits	Buckling curve
Rolled I-sections	$b/b \leq 2$	a
	$b/b > 2$	b
Welded I-sections	$b/b \leq 2$	c
	$b/b > 2$	d
Other cross-sections	-	d

Table 6.3: Recommended values for imperfection factors for lateral torsional buckling curves

Buckling curve	a	b	c	d
Imperfection factor α_{LT}	0.21	0.34	0.49	0.76

+

$$\alpha_{LT} := 0.21$$

$$\phi_{LT} := 0.5 \cdot (1 + \alpha_{LT} \cdot (\lambda_{LT} - 0.2) + \lambda_{LT}^2) = 1.003$$

$$\chi_{LT} := \frac{1}{\phi_{LT} + \sqrt{\phi_{LT}^2 - \lambda_{LT}^2}} = 0.718$$

$$M_{b,rd} := \chi_{LT} \cdot W_y \cdot \frac{f_y}{\gamma_{m1}} = 160.029 \text{ kN} \cdot \text{m}$$